Aus dem Lehrstuhl für Humangenetik
Prof. Dr. Bernhard Weber
der Fakultät für Medizin
der Universität Regensburg

Generation of Retinal Organoid-Retinal Pigment Epithelium Cocultures

Inaugural – Dissertation
zur Erlangung des Doktorgrades
der Medizin

der
Fakultät für Medizin
der Universität Regensburg

vorgelegt von
Sofiia Bondarenko

2023

Aus dem Lehrstuhl für Humangenetik
Prof. Dr. Bernhard Weber
der Fakultät für Medizin
der Universität Regensburg

Generation of Retinal Organoid-Retinal Pigment Epithelium Cocultures

Inaugural – Dissertation
zur Erlangung des Doktorgrades
der Medizin

der
Fakultät für Medizin
der Universität Regensburg

vorgelegt von
Sofiia Bondarenko

2023

Dekan:	Prof. Dr. Dirk Hellwig
1. Berichterstatter:	Prof. Dr. Bernhard Weber
2. Berichterstatter:	Prof. Dr. Klaus Stark
Tag der mündlichen Prüfung:	18.12.2023

Table of contents

1 Zusammenfassung

Die Forschung an Erkrankungen der menschlichen Netzhaut steht stets vor der Herausforderung, ein wissenschaftliches Model zur Verfügung zu haben, das vielfältige Eigenschaften der menschlichen Netzhaut möglichst realistisch nachahmen kann. Als vor einigen Jahren Protokolle für Differenzierung von retinalen Organoiden (ROs) aus humanen induzierten pluripotenten Stammzellen (hiPSCs) publiziert wurden, hat die wissenschaftliche Welt sie als Durchbruch in der Netzhautforschung angesehen. ROs enthalten alle Hauptzelltypen der menschlichen Netzhaut und erinnern in ihrer Struktur prinzipiell an dieses Gewebe *in vivo*. Sie weisen jedoch erhebliche Einschränkungen auf. Gerade für Forscher, die das Zusammenspiel von Photorezeptoren und retinalem Pigmentepithel (RPE) untersuchen wollen, stellen der fehlende physiologische Kontakt zwischen diesen Zelltypen und unterwickelte Außensegmente der Photorezeptoren einen großen Nachteil der ROs als Modellsystem dar.

Diese Dissertation erarbeitete ein modifiziertes Protokoll zur Differenzierung von ROs, mit einer gleichzeitigen Erzeugung von hochqualitativem RPE, genannt bRPE. Die hiPSCs, die sich nicht zu Organoiden differenzierten, dienten hierbei als Grundlage für die RPE-Differenzierung mittels Zellmedium-Zusatzstoff Nikotinamid. Das adaptierte Protokoll wurde mit drei hiPSC-Zelllinien, die von gesunden Spendern stammen, getestet. In jeder Differenzierung konnten pigmentierte Zellen gewonnen werden, die eine RPE-typische Morphologie aufwiesen und spezifische RPE-Zellproteine in den immunzytochemischen Untersuchungen exprimierten. Die signifikant höhere Expression von drei RPE-Markern im Vergleich zu hiPSC konnte mittels qRT-PCR (*Englisch: quantitative reverse transcriptase polymerase chain reaction*) nachgewiesen werden. Diese Ergebnisse deuten darauf hin, dass unser modifiziertes Protokoll zu erfolgreicher und zuverlässiger Differenzierung von RPE führt.

In einem weiteren Teilprojekt wurden zwei Bedingungen für gemeinsame Kultivierung von ROs und bRPE-Zellen in drei Experimenten untersucht. Zweimal wurden ROs mit bRPE in Suspension kultiviert. Viele bRPE-Zellen lösten sich innerhalb weniger Tage von der RO-Oberfläche, obwohl zwischen ihnen physischer Kontakt bestand. Im dritten Experiment wurden ROs auf der Monoschicht aus den bRPE-Zellen kultiviert. Die ROs hafteten vorübergehend am bRPE, lösten sich aber während des Ernteprozesses. Dennoch färbten sich die bRPE-Zellen positiv für Rhodopsin, einen Marker für Außensegmente von Photorezeptoren. Diese Erkenntnis weist auf eine funktionelle Beziehung zwischen Organoiden und bRPE hin. Durch

unsere Versuche, ROs mit bRPE zu kultivieren, wurde eine solide Grundlage für zukünftige Experimente geschaffen. Die Etablierung von einem robusten Modell für gemeinsame Kultivierung dieser Zellarten würde ROs näher an den physiologischen Zustand bringen und ihre Anwendungen in der Netzhautforschung wesentlich erweitern.

Zusätzlich untersuchte dieses Projekt hiPSC-Klone, die mit CRISPR/Cas9-Methode behandelt wurden, um gezielt DNA-Veränderungen im *Retinitis Pigmentosa 1 Axonemal Microtubule Associated (RP1)* Gen zu induzieren. Mutationen im *RP1*-Gen sind eine häufige Ursache für Retinitis pigmentosa, eine genetische Erkrankung, die mit der Degeneration von Photorezeptoren verbunden ist. Es wurde festgestellt, dass ein hiPSC-Klon eine neuartige homozygote Mutation im *RP1*-Gen trägt, die aller Voraussicht nach zum *RP1*-Knockout-Phänotyp führt. Die zukünftige Differenzierung von ROs aus diesem hiPSC-Klon könnte einen Ausgangspunkt für die Untersuchung der Funktionen des RP1-Proteins und der Pathogenese der Retinitis pigmentosa in diesem faszinierenden Netzhautmodel bieten.

2 Introduction

A healthy visual system is essential for daily life. It affects our ability to interact with the environment and perform critical tasks such as reading and writing. For over 100 years, researchers have been studying disorders of this system, which can severely impact one's quality of life.

Visual perception starts in the eyes, highly complex organs that detect light stimuli and convert them into electrical signals. The light-sensitive part, called the retina, is located at the back of the eye. Countless patients worldwide are affected by retinal diseases that impair their vision. Therefore, it is crucial to have dependable scientific models to advance our understanding of disease pathogenesis and drug testing for these conditions.

This project focuses on studying retinal organoids (ROs) as a model for the human retina. The protocol to differentiate ROs from human induced pluripotent stem cells (hiPSCs) was modified to counteract one of the significant limitations ROs as a retina model carry: the absence of the retinal pigment epithelium (RPE) layer. In addition, the coculture conditions for the generated ROs and RPE were assessed. In the final section of this study, we analyzed hiPSCs that had undergone the CRISPR/Cas9 treatment to identify novel mutations in the targeted *Retinitis Pigmentosa 1 Axonemal Microtubule Associated (RP1)* gene.

2.1 Human Retina

2.1.1 Structure and Embryogenesis of the Human Retina

In the retina, light stimuli are perceived, processed, and, ultimately, conducted to the brain. Anatomically, the retina comprises three layers housing specialized neurons: the ganglion cell (GCL), inner nuclear (INL), and outer nuclear (ONL) layers (Figure 1). The inner (IPL) and outer plexiform (OPL) layers, consisting of synapses between retinal neurons, are situated between the nuclear layers. The ONL houses the cell bodies of light-sensing cells, named photoreceptors, while their distal parts are situated in the photoreceptor layer (PL). RPE cells adjacent to the neural retina form the outermost layer. The INL contains interneuron cell bodies of three types: bipolar, horizontal, and amacrine neurons. Amacrine and horizontal cells modulate retinal response to light, while bipolar neurons transmit signals from photoreceptors to ganglion cells. The somata of ganglion cells are situated in the GCL of the retina. Their axons form the nerve fiber layer (NFL) and converge at the optic disc to create the optic nerve, transmitting electrical signals to the brain. Additionally, the retina contains specialized neural

support cells called the Mueller glial cells, which stretch through all three nuclear layers. These cells facilitate the functioning and metabolism of retinal neurons (reviewed in (1)).

The retina belongs to the tissues with a high metabolism and relies heavily on the circulatory system to deliver oxygen and nutrients. Two vascular networks supply it: the anterior retinal and posterior choroidal vessels nurture the innermost retinal cells and the outer layers, respectively (2). It is important to note that the retinal neurons are protected from direct contact with the circulatory system. It is due to the blood-retinal barrier, formed by the tight junctions between the RPE and endothelial cells, and basement membranes (reviewed in (3)).

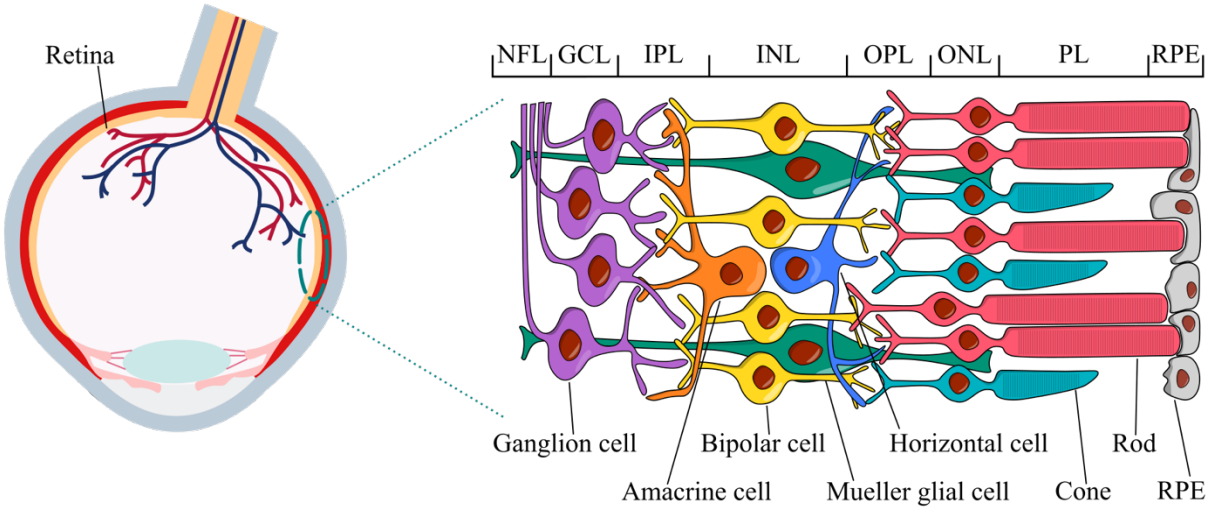

Figure 1. Structure of the human retina. The retina is the innermost sheet of the eyeball. It consists of specialized neurons organized into separate layers. The RPE is the outermost layer of the retina and is located close to the photoreceptors. The ONL contains photoreceptor cell bodies, while interneurons are situated in the INL. The GCL houses the ganglion cells, which transmit signals from the retina to the brain. The synapses between retinal neurons lie in the OPL and IPL. Mueller glial cells extend through all nuclear layers. This figure was modified after (4,5).

To understand retinal disease pathogenesis, the knowledge of not only the structure of the retina but also its embryonic development is essential. The retina arises from a protuberance of the diencephalon, termed optic vesicle, which extends to the lens placode (Figure 2) (reviewed in (6)). From the lens placode emerges the lens, a transparent structure that focuses light onto the retina. A coordinated invagination of the optic vesicle results in a bilayered optic cup containing an inner layer of neural retinal precursor cells and an outer layer of RPE precursors. The retinal cell types arise in sequential order (7–9). Retinal ganglion cells differentiate first, followed by photoreceptors, amacrine, and horizontal cells. The final emerging cell types are bipolar and Mueller glial cells.

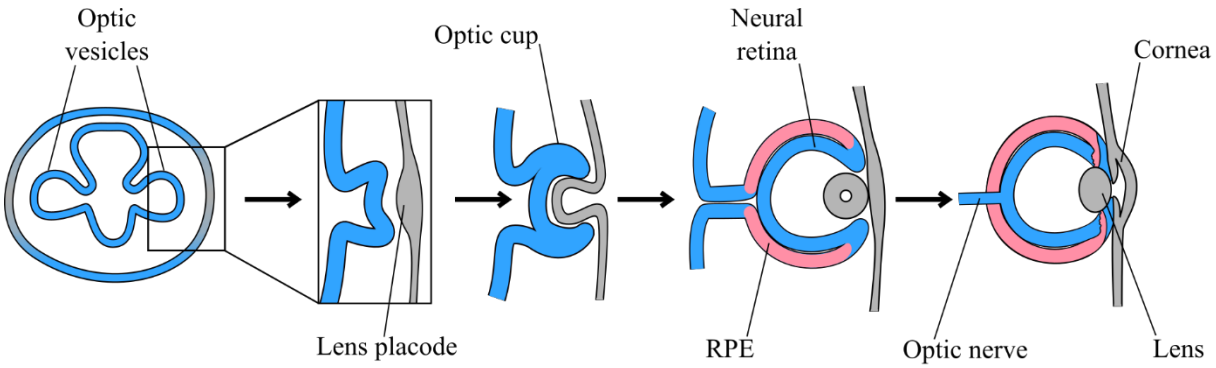

Figure 2. Retinal development. The human retina develops from the optic vesicle, which arises as an evagination of the diencephalon. The optic vesicle comes into close contact with the lens placode, which matures to the lens. The optic vesicle invaginates, generating a bilayered optic cup. The neural retina develops from the inner layer, while the RPE derives from the outer layer of the optic cup. This figure was modified after (10).

For this project, photoreceptors, which convert light stimuli into electrical signals, are the cells of the highest importance. Therefore, the upcoming chapter will delve deeper into the structure of photoreceptors and their role in visual perception.

2.1.2 Human Photoreceptors

Photoreceptors are the most critical light-sensing cells of the retina. They can be subcategorized into rods and cones based on the light conditions they can detect (11). Rod photoreceptors, incapable of discerning colors, facilitate vision at low light levels. In contrast, cone photoreceptors are responsible for high-resolution and color vision, being active only under bright light conditions. The human retina contains twenty times as many rods as cones, while the distribution of both photoreceptor types through the retina is not homogenous (12). The fovea, a region of the human retina that conveys high-acuity central vision, is exclusive to cones. Their number decreases radially from it, so the peripheral retina houses only rods.

All photoreceptors share the same basic structure with slight morphological differences between rods and cones (Figure 3). They can be broadly divided into four parts: synaptic terminal, cell body, and inner and outer segment. The inner segment (IS) lies distal from the cell body and is a mitochondria-rich, metabolically active part of the photoreceptors. It is connected to the outer segment (OS) via the axoneme in the connecting cilium (reviewed in (13)). In its proximal part, the axoneme comprises nine circularly arranged microtubule doublets, replaced by nine single microtubules in the distal portion. Along these microtubules, motor proteins transport various molecules, synthesized in the IS but functional in the OS.

The main structural difference between rods and cones is their OS morphology (Figure 3) (11). The OSs of rods have a cylindrical shape and are made up of stacked equally sized

membranous discs enclosed by the cell membrane. In the cone OSs, the stacks of membranous discs are formed through multiple invaginations of the cell membrane. The discs become smaller at the tip of the OS, creating a cone-shaped appearance. This complex structure facilitates visual function, namely a crucial process called phototransduction.

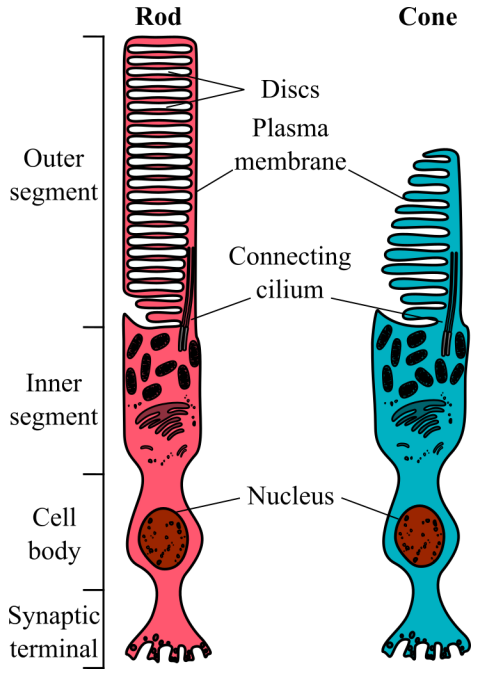

Figure 3. Photoreceptor structure. There are two types of photoreceptor cells in the human retina: rods and cones. Both types can be divided into the cell body with the nucleus, synaptic terminal, IS, and OS. The morphology of the OSs differs between rods and cones. The membrane discs in rods are all the same size and separated from the cell membrane. In cones, the discs are formed by cell membrane invaginations, and they become smaller at the tip of the OSs. The figure was modified after (14).

Phototransduction, or conversion of a light stimulus to an electric impulse, occurs in the OS membrane discs. Within these membranes, a photoreactive chromophore, named 11-cis-retinal, is incorporated, which is bound to a photosensitive protein (reviewed in (15)). The family of photosensitive proteins is referred to as opsins, and the photoreceptor subcategories contain slightly different opsin varieties. Rod photoreceptors express rhodopsin, whereas cones express red, green, or blue opsins, depending on their transmission wavelength. Exposure to light triggers the isomerization of 11-*cis*-retinal to all-*trans*-retinal, which induces a conformational change of the attached opsin. As a result of several intermediate steps, the sodium channels close, photoreceptors hyperpolarize, and the release of neurotransmitter glutamate at the synapses with retinal interneurons decreases (reviewed in (16)).

It is vital to maintain the cellular homeostasis of the photoreceptors for the phototransduction cascade to occur. Direct exposure to light causes photooxidative stress and

leads to the accumulation of toxic substances in the photoreceptor OSs (reviewed in (17)). To preserve optimal function, continuous renewal of the OS proteins and membranes and elimination of harmful wastes is essential. The regeneration of the OS components is ensured through the constant replacement of the membrane discs: the oldest discs are shed at the OS tip, while the new ones are assembled at the base (reviewed in (18)). This process and many others are facilitated by the RPE cells, which support photoreceptors in their functions.

2.1.3 Photoreceptor-RPE System

The RPE is a single layer of pigmented cells that play an essential role in visual perception. Their primary objective is to maintain the functionality of rods and cones. The RPE provides photoreceptors with nutrients and oxygen from the blood since the neural retina is isolated from the circulatory system by the blood-retinal barrier. Tight junctions between neighbouring RPE cells hinder the unregulated movement of molecules (reviewed in (19)). This allows for controlled transportation of nutrients to the retina and waste elimination (reviewed in (20)). Besides, tight junctions play a role in the polarization of RPE by dividing the cell membrane into apical and basolateral sides, which face photoreceptors and choroidal blood vessels, respectively.

In order to maintain the homeostasis of the photoreceptors, RPE cells encapsulate a closed subretinal space where the photoreceptor OSs protrude (reviewed in (20,21)). The extracellular matrix (ECM) and the RPE apical microvilli strengthen the adhesion between these cell types. Additionally, the RPE secretes soluble factors indispensable for photoreceptor development and spatial organization (22–24). Phagocytosis of shed OS membrane discs and recycling of photopigments like 11-*cis*-retinal are further essential functions of the RPE. The regeneration of the 11-*cis*-retinal from the bleached all-*trans*-retinal is achieved through the visual cycle, which involves various enzymes and intermediates (reviewed in (18)). Moreover, the RPE reduces oxidative stress on retinal neurons and improves visual acuity by absorbing stray light with its pigmented granules (reviewed in (17)).

Due to the close functional relationship between RPE and photoreceptors, disorders of either cell type can cause the degeneration of the other. The detrimental repercussions of this co-dependency are responsible for multiple conditions involving visual acuity deterioration or even blindness. Inherited retinal diseases (IRDs) are genetic disorders that affect the photoreceptors-RPE system. The most common IRD is retinitis pigmentosa (RP) (35-61%) (25–27). Other IRDs include cone-rod dystrophy (4%), Leber congenital amaurosis (LCA) (5,2-9%), and Stargardt macular dystrophy (6,5-21%) (25–27).

2.2 Retinitis Pigmentosa

RP (OMIM # 268000) is the most common monogenic IRD, with a prevalence of approximately 1:4000 (reviewed in (28)). It is the primary cause of blindness in individuals under the age of 60 (reviewed in (29)). RP is characterized by the degeneration of primarily rod photoreceptors, followed by cones (reviewed in (28)).

An early symptom of RP is night blindness (nyctalopia), which usually occurs in childhood or early adolescence. Years later, patients experience a deterioration of their peripheral vision. This starts with many isolated scotomas (blind spots) in the mid-periphery of the visual field, which later confluence to a ring scotoma (reviewed in (28)). The ring's outer edge expands rapidly to the periphery, while the central vision stays preserved until the late stages of disease. This process results in a condition referred to as tunnel vision (reviewed in (30)). During this stage, most patients cannot move around independently but retain the ability to perceive light or even read. Eventually, many affected individuals are rendered legally blind. Despite recent advancements in therapeutic strategies, no cure is currently available for patients with RP (reviewed in (31)).

Genetic counseling is highly recommended for individuals with a clinically diagnosed or suspected RP (reviewed in (28)). Non-syndromic RP, which affects only the retinal tissue, can be inherited in multiple modes: X-linked (6-17% of patients), autosomal-dominant (8-35%), or autosomal-recessive (16-45%) (32–35). In some cases, the mode of inheritance is not immediately apparent as the index patient is the only affected family member. In such situations, patients are said to have simplex RP (23-50%) (32–35). To date, causal mutations for non-syndromic RP have been identified in more than 90 genes (36). These genes often play vital roles in photoreceptor and RPE functions, like phototransduction or visual cycle (reviewed in (28)). Despite significant progress in genetic testing, the pathological variant cannot be detected in 40-50% of patients with a clinical diagnosis of RP (30,37,38). Verbakel et al. conducted a review on the distribution of RP-causing genes (28). They reported mutations in the *RP1* gene as a frequent cause of non-syndromic RP. Next, we will explore the function of the *RP1* gene and the potential effects of its mutations on the photoreceptor-RPE system.

2.2.1 *RP1* Gene

The *RP1* gene was first identified to cause autosomal-dominant retinitis pigmentosa type 1 in 1999 (39). Mutations in this gene are responsible for 3,5-10,5% of autosomal-dominant and 1% of autosomal-recessive RP cases (37,39–42). Recently, the *RP1* mutations were also described to cause autosomal-recessive macular and cone-rod dystrophy (43).

The *RP1* gene consists of 4 exons, while only the latter three are transcribed to the mRNA (39). Autosomal-dominant *RP1* mutations are clustered in the short region at the 5'-end of the exon 4, most resulting in a premature stop codon (44). Usually, the cells degrade mRNA that contains premature stop codons via nonsense-mediated decay (reviewed in (45)). In this way, possible negative repercussions of truncated proteins would be reduced. However, if the premature stop-codon is in the final exon, like in this case, the mRNA will be translated as usual (46). A previous publication has confirmed that truncated RP1 protein can be found within photoreceptor OSs (47).

The *RP1* gene encodes for a photoreceptor-specific protein found in the proximal part of the OS (47,48). The RP1 protein contains a microtubule-binding domain and is associated with the photoreceptor axoneme. A previous paper reported that it plays a role in stabilizing and regulating the length of the axoneme (49). Moreover, the RP1 protein is indispensable for the correct orientation of the OS membrane discs. Studies from the early 2000s have demonstrated that homozygous *RP1* mutations result in the disorganization of the OS discs and rod photoreceptor degeneration in mice (47,48). Despite this early success, little progress has been made in understanding the pathogenesis of autosomal-dominant or recessive *RP1* disease within the past few years. This situation highlights the need for innovative methods to investigate RP.

2.3 Retinal Model Systems

Studying the pathophysiology of human retinal disease has been challenging because of the limitations of the currently available model systems, which include animal models, post-mortem and fetal samples, and stem cell-based cultures. Often used animal models, for example, rodents, can reproduce the phenotype of certain retinal disorders. Still, not all findings are transferable to humans due to differences in eye size, functioning of photoreceptors, retinal vasculature, or different genetic backgrounds (reviewed in (50)).

Another way to study retinal disease is by analyzing human post-mortem specimens. The retinal explants contain all important cells and preserve the *in vivo* structure of the retina. Studying human tissue has the advantage of eliminating inter-species variability, but it is also connected with its challenges. Human post-mortem samples are difficult to obtain, especially since the retina remains viable only briefly after circulatory arrest. Moreover, post-mortem tissue usually represents only advanced disease stages, and observation of disease progression is impossible (reviewed in (51)). While adult tissue is highly limited, human fetal and early

postnatal tissue samples are unreachable to researchers worldwide, as they are subject to strict legal and ethical requirements (52).

Considering the aspects mentioned above, a retinal model that is easily accessible and allows researchers to work with human samples for an extended time may lead to progress in studying IRDs. The discovery of a stem cell-derived technique granted scientists access to developing human tissue in the laboratory setting, a long-awaited breakthrough in retinal research.

2.3.1 Retinal Organoids

A promising retinal model system has ignited a new wave of research within the past decade. In 2007, the revolutionary finding that adult somatic cells can be reprogrammed to regain pluripotency was published (53). These pluripotent cells were termed hiPSCs. They had the potential to differentiate into any of three germ layers (ectoderm, endoderm, mesoderm), similar to human embryonic stem cells (hESCs) (53,54).

It was theorized that hiPSCs could be differentiated into retinal cells. The next challenge for researchers was identifying the precise triggers to induce retinal differentiation *in vitro*. Early findings focused on the differentiation of hiPSCs to RPE cells and photoreceptors in two-dimensional (2D) adherent cultures (55,56). Protocols that produced cells exhibiting key characteristics of RPE were quickly established, whereas progress with the photoreceptor differentiation stagnated (reviewed in (50)).

As photoreceptor loss is an integral phenotypic feature of many IRDs, creating more efficient protocols to produce and maintain photoreceptors *in vitro* was highly desirable. The critical development, which revitalized photoreceptor differentiation research, was a finding from brain researcher Sergiu Pașca. He discovered that hiPSC-derived neurons withered in the 2D adherent culture but thrived as 3D cellular aggregates (57). These aggregates contained multiple neuronal cell types and had a similar structure to the human brain, so they were later named brain organoids (reviewed in (58)).

For retinal researchers, this technique proved to be the missing piece required to culture hiPSC-derived neural retinal cells *in vitro,* leading to the birth of 3D aggregates named ROs (Figure 4A) (59). It was demonstrated that the cellular development of ROs follows a characteristic time-dependent sequence comparable with the embryonic formation of the native retina (60,61). ROs develop the same cell types as the neural retina, and their stratification resembles the native tissue (61–63). Moreover, synaptic structures were detected in the putative OPL and IPL of ROs via electron microscopy and immunocytochemistry (ICC) (60,64).

These characteristics have opened a new avenue of research, as ROs have tremendous potential as a scientific model. Soon, the first studies using ROs as an IRD model were published (65,66).

2.3.2 ROs as Retinal Disease Model

Multiple studies have already used ROs as IRD models for studying disease phenotypes and therapeutic strategies. For example, ROs successfully recapitulated the pathogenesis of RP type 2 (65). This X-linked RP type is caused by mutations in the *Retinitis Pigmentosa 2 Activator of ARL3 GTPase (RP2)* gene. The RP2 protein is required for ciliary function and photoreceptor preservation *in vivo*. In ROs derived from patient hiPSCs, rod photoreceptor cell death was detected between day 150 and 180 in culture. Pursuing treatment, at day 140, researchers transfected affected ROs with adeno-associated virus vectors containing the wild-type *RP2* gene (65). Sufficient transfection of rods and cones was confirmed, and a decline in rod photoreceptor cell death was observed in the treated ROs.

In another study, organoids were generated from an LCA patient with a homozygous mutation in the *Aryl Hydrocarbon Receptor-Interacting Protein-Like 1 (AIPL1)* gene (66). The *AIPL1* gene encodes a photoreceptor-specific chaperone, which stabilizes the phosphodiesterase 6, the key enzyme of the phototransduction process. In LCA patients, photoreceptors degenerate during the first year of life, causing severe vision impairment (reviewed in (67)). Notably, there was no observed photoreceptor degeneration in the patient-derived ROs. Despite the reduction in AIPL1 expression, they exhibited similar morphology to control organoids (66). The absence of the LCA phenotype may be caused by an inactive phototransduction cascade in ROs, so the photoreceptor cell death was not triggered. These results suggest that using ROs as a model to study IRDs caused by gene mutations in the phototransduction cascade may not always be reasonable.

2.3.3 RO Limitations and Challenges

While ROs provide a unique opportunity to study human retinal tissue, they are burdened by some intrinsic limitations. Firstly, the differentiation time of ROs is very long. Scientists have cultivated ROs and brain organoids for up to two years (60,68,69). This research indicates that organoids mature along a similar timeline as human embryological *in vivo* development (61,70). Therefore, a 3-month-old RO, for example, most closely resembles the retina of a 3-month-old fetus. Moreover, this relatively slow development can be derailed at any time through bacterial or mycotic contamination of organoids, rendering them unusable. Researchers must follow strict cell culture guidelines to avoid contaminating the ROs.

The further drawback of ROs is that they do not develop endothelial cells, leading to a lack of blood vessel-like structures (reviewed in (50)). Consequently, the RO inner layers receive nutrients and oxygen through diffusion. With the steady growth of organoids, the inner cells become undersupplied, which may be one of the reasons causing the degeneration of the inner retinal layers in long-term culture (61,71).

Researchers using ROs to study IRDs face a challenge due to the absence of fully developed rods and cones (Figure 4A). It was shown that RO photoreceptors usually form only short OSs with incorrectly stacked membrane discs (60,61,64,72). Nevertheless, ROs contain rhodopsin-positive rods and red, green, and blue opsin-positive cones, which are mostly evenly distributed across organoids (60). Zhong et al. investigated the light responsiveness of these photoreceptors via perforated patch recordings in the voltage clamp mode (61). Two of the 13 analyzed cells reacted to light stimuli. The light responses resembled the ones in the native retina, although they were much weaker.

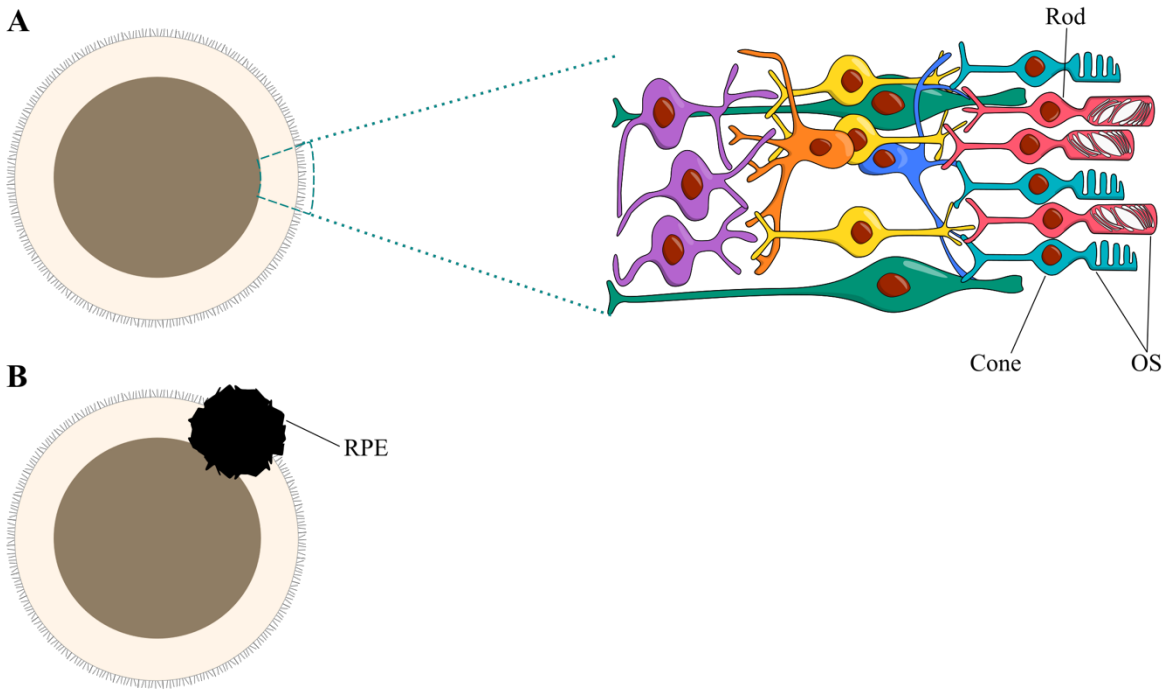

Figure 4. RO structure. (A) A schematic picture of a RO illustrates its bright outer part, corresponding to the developing retina, and darker inner part. The magnification shows that RO photoreceptors contain nascent OSs with incorrectly stacked membrane discs. The RPE monolayer is absent in ROs. **(B)** Some ROs carry clusters of RPE cells, which have no contact with photoreceptors. This figure was modified after (4,5).

A probable cause for underdeveloped photoreceptor OSs could be a lack of physiological relationship with RPE (reviewed in (73)). During retinogenesis, the optic vesicle invaginates to produce a bilayered optic cup (reviewed in (6)). The cells in the outer layer

differentiate to RPE, whereas retinal neurons, including photoreceptor cells, emerge from the inner layer. So far, this process has rarely been recapitulated during RO maturation (59,63). The RO differentiation mainly gives rise to RPE patches hanging on the tip of some ROs (Figure 4B) (60,61,72). As a result, maturing rods and cones are deprived of physical contact with RPE cells and soluble molecules they secrete. Moreover, the subretinal space is absent, and photoreceptors are directly exposed to the feeding medium. As RPE cells are essential for phototransduction in terms of the visual cycle and phagocytosis of OS membrane discs, they are likely indispensable for the generation of fully functioning photoreceptors in ROs. Also, considering the importance of the photoreceptor-RPE intimate relationship for IRD pathogenesis, the next hurdle for researchers will be developing methods to bring RO photoreceptors into close physical contact with RPE cells.

Nonetheless, various alternative approaches have been examined to enhance the photoreceptor maturation in ROs. Increased numbers of rods and S-cones (sensitive to light of short wavelength) have been shown to result from the administration of retinoic acid (RA) and triiodothyronine during days 90-120 of differentiation (74). Moreover, accelerated and improved development of all retinal cell types in the ROs, derived from mouse embryonic stem cells, was described when organoids were cultivated in rotating-wall vessel bioreactors (75).

2.3.4 RO-RPE Coculture

A promising way to replicate the interaction between photoreceptors and RPE cells *in vitro* is by coculturing both tissues. Although RO differentiation protocols were published many years ago, only a few publications investigate an RO-RPE coculture system (76,77). In one study, hiPSC-derived ROs were brought in contact with RPE cells from murine explants (76). This method had some drawbacks, primarily because it involved using cells from two different species. Nevertheless, the researchers reported several promising effects of the coculture system. They observed that the photoreceptor development in the ROs was accelerated. Of note, control ROs eventually caught up with the number of photoreceptors in the cocultured organoids (76). Also, this study showed that direct physical contact was essential for accelerated photoreceptor differentiation, as the RPE-conditioned medium did not affect RO development.

Another report of an RO-RPE coculture system described a far more sophisticated approach. This project was performed by a research group specializing in the culture of hiPSC-derived tissues on microfluidic chips (77). These chips enable the unidirectional flow of media, thereby mimicking the vasculature system. In this publication, the researchers seeded RPE cells on the chip and introduced an organoid a few days later. After one week, they harvested the

coculture system and found multiple exciting improvements to the photoreceptors in the ROs. The RO-RPE coculture increased the formation of the photoreceptor OS, and the phagocytosis of the OS discs by the RPE was confirmed. A protective effect of the RPE layer was revealed, as gentamicin-induced cell death was prevented in the ROs (77). This coculture strategy addressed some RO limitations, but its complexity hinders its adoption by other researchers.

Furthermore, the RPE used in this publication was harvested from the RPE clusters attached to the ROs. This approach produces only a small quantity of RPE cells, severely limiting their applications. Besides, the separation of RPE clumps required their manual excision from the ROs, thereby jeopardizing the health and integrity of the organoids (77). Thus, scientists interested in researching an RO-RPE system would greatly benefit from a reliable method to generate and expand high-quality RPE cells from an RO differentiation protocol.

2.4 Aim of this Study

HiPSC-derived ROs have tremendous potential as retinal disease and drug screening models, but their application has some limitations, as described earlier. One major drawback is the lack of physiological contact between RO photoreceptors and RPE cells. A fascinating approach to address this concern would be to coculture ROs with RPE. Creating such a model is highly desirable to diversify the utility of ROs as an RP model. However, an efficient and reproducible method to generate high-quality RPE cells must be devised before a coculture system can be approached. HiPSC-derived RPE differentiation protocols are well-established, but the inductive queues in these protocols differ greatly from those during RO differentiation.

The thesis is comprised of three main sections. Firstly, the project investigated adjusting the existing protocol to obtain RPE cells from initial RO differentiation. To reach this goal, the hiPSCs that had not initially developed to ROs were cultured separately for several more weeks. The differentiating cells were tested for expression of characteristic RPE markers using ICC and quantitative reverse transcriptase polymerase chain reaction (qRT-PCR). The second main objective of this thesis was to investigate two RO-RPE coculture conditions. Finally, hiPSC single clones previously treated with the CRISPR/Cas9 system targeting the *RP1* gene were analyzed for generated DNA alterations.

3 Materials

3.1 Cell Lines

Table 1. hiPSC lines used in the study.

Cell line	Pseudonym	Clones	Clone pseudonym	Tissue of origin
NG050912	hiPSC line 1	3	Clone A	Adult skin fibroblasts
		2	Clone B	
MK270413	hiPSC line 2	27	Clone A	Adult skin fibroblasts
		26	Clone B	
NJ250216	hiPSC line 3	105	Clone A	PBMC
		111	Clone B	
MK161019B				With CRISPR/Cas9 treated hiPSCs from cell line MK270413 Clone 26

PBMC: peripheral blood mononuclear cells. All cell lines were generated at the Institute for Human Genetics, University of Regensburg, Germany.

3.2 Oligonucleotides

All oligonucleotides were obtained from Metabion International AG, Planegg/Steinkirchen, Germany.

3.2.1 Single-Guide RNAs

Table 2. Single-guide RNAs (sgRNA) used in the study.

sgRNA	Sequence (5´ - 3´)
SZ_RP1_KO_7F	TAATACGACTCACTATAGgcacagcatcacgcgcctgg
SZ_RP1_KO_7R	TTCTAGCTCTAAAACccaggcgcgtgatgctgtgc

Upper-case letters stay for T7-promoter.

3.2.2 Primers for PCR and Sanger Sequencing

Table 3. Primers used for PCR and Sanger sequencing.

Primer	Sequence (5´ - 3´)
RP1_Ex2.1_EcoR1_F	GAATTCtgcattagtattaccatgtattcgc
RP1_Ex2.2_BamHI_R	GGATCCcacacgaatccaattagtag

Upper-case letters mark cleavage site for BamHI restriction enzyme.

3.3 Antibodies

Table 4. Primary antibodies used in the study.

Antigen	Clonality	Species	Dilution	Application	Company
BEST1	pAb	rabbit	1:250	ICC	immunoGlobe GmbH, Himmelstadt, Germany
BEST1	mAb	mouse	1:500	ICC	Abcam, Cambridge, UK

hNANOG	mAb	mouse	1:300	ICC	Thermo Fisher Scientific, Waltham, MA, USA
hSSEA3	mAb	rat	1:300	ICC	Thermo Fisher Scientific, Waltham, MA, USA
Ki67	pAb	rabbit	1:100	ICC	Abcam, Cambridge, UK
Na^+/K^+-ATPase1 (ATP1-A1)	pAb	rabbit	1:100	ICC	Proteintech Group, Rosemont, IL, USA
Recoverin	pAb	rabbit	1:1000	ICC	Merck KGaA, Darmstadt, Germany
Rhodopsin	mAb	mouse	1:1000	ICC	Robert Molday, Vancouver, BC, Canada
RPE65	mAb	mouse	1:500	ICC	Abcam, Cambridge, UK
TRA 1-60	mAb	mouse	1:300	ICC	Abcam, Cambridge, UK
Zonula occludens -1	pAb	rabbit	1:500	ICC	Thermo Fisher Scientific, Waltham, MA, USA

pAb: polyclonal antibody; mAb: monoclonal antibody.

Table 5. Secondary antibodies used in the study.

Name	Company
Alexa Fluor® 488 goat anti-rabbit IgG (H+L)	Thermo Fisher Scientific, Waltham, MA, US
Alexa Fluor® 568 goat anti-mouse IgG (H+L)	Thermo Fisher Scientific, Waltham, MA, US
Alexa Fluor® 594 goat anti-mouse IgG (H+L)	Thermo Fisher Scientific, Waltham, MA, US
Alexa Fluor® 488 goat anti-rat IgG (H+L)	Thermo Fisher Scientific, Waltham, MA, US

IgG: immunoglobulin G.

3.4 Enzymes and Enzymatic Buffers

Table 6. Enzymes used in the study.

Enzyme	Company
Antarctic Phosphatase	New England Biolabs, Ipswich, MA, USA
Dispase in DMEM/F12	STEMCELL Technologies Canada Inc., Vancouver, BC, Canada
Exonuclease I	Affymetrix, USB Products, Santa Clara, CA, USA
GoTaq® DNA-Polymerase	Promega Corporation, Madison, WI, USA
Pronase E (from Streptomyces griseus)	Merck KGaA, Darmstadt, Germany
TrypLE™ Select (1x)	Thermo Fisher Scientific, Waltham, MA, USA

Table 7. Enzymatic buffers used in the study.

Buffer	Company
5x GoTaq® Reaction Buffer, green	Promega Corporation, Madison, WI, USA
5x Sequencing Buffer	Thermo Fisher Scientific, Waltham, MA, USA

3.5 Reaction Kits

Table 8. Reaction kits used in the study.

Kit	Company
Big Dye Terminator v. 3.1. Cycle Sequencing Kit	Thermo Fisher Scientific, Waltham, MA, USA

PureLink™ RNA Mini Kit	Thermo Fisher Scientific, Waltham, MA, USA

3.6 Chemicals

Table 9. Chemicals used in the study.

Chemical	Company
(-)-Blebbistatin	Cayman Chemical, Ann Arbor, MI, USA
4′,6-diamidino-2-phenylindole (DAPI)	Thermo Fisher Scientific, Waltham, MA, USA
Agarose (Biozym LE)	Biozym Scientific GmbH, Hessisch Oldendorf, Germany
All-*trans* retinoic acid	Cayman Chemical, Ann Arbor, MI, USA
Boric acid	Fisher Scientific UK Ltd, Loughborough, UK
Bromophenol Blue sodium salt	Sigma-Aldrich, St. Louis, MO, USA
Corning® Matrigel® Growth Factor Reduced (GFR) Basement Membrane Matrix	Corning, NY, USA
Corning® Matrigel® hESC-qualified Matrix	Corning, NY, USA
Dako Fluorescence Mounting Medium	Agilent Technologies, Inc., Santa Clara, CA, USA
DEPC	AppliChem GmbH, Darmstadt, Germany
Dimethylsulfoxide (DMSO)	Carl Roth GmbH + Co. KG, Karlsruhe, Germany
DMSO, 100%	New England Biolabs, Ipswich, MA, USA
dNTPs	Genaxxon Bioscience, Ulm, Germany
Ethanol absolute	Sigma-Aldrich Co., St. Louis, MO, USA
Ethidium bromide solution 0.07%	AppliChem GmbH, Darmstadt, Germany
Ethylenediaminetetraacetic acid (EDTA)	Merck KGaA, Darmstadt, Germany
Heparin sodium salt from porcine intestinal mucosa	Sigma-Aldrich Co., St. Louis, MO, USA
Hi-Di™ Formamide	Thermo Fisher Scientific, Waltham, MA, USA
Human BMP4 Recombinant Protein (BMP4)	Thermo Fisher Scientific, Waltham, MA, USA
Hydrogen peroxide solution (34.5 – 36.5%)	Sigma-Aldrich Co., St. Louis, MO, USA
Mycoplasma removal agent	Bio-Rad Laboratories GmbH, Feldkirchen, Germany
Nicotinamide, suitable for cell culture	Sigma-Aldrich Co., St. Louis, MO, USA
Paraformaldehyde (PFA), 4% in phosphate-buffered saline (PBS)	Thermo Fisher (Kandel) GmbH, Kandel, Germany
Potassium chloride (KCl)	Merck KGaA, Darmstadt, Germany
Potassium dihydrogen phosphate (KH_2PO_4)	Merck KGaA, Darmstadt, Germany
Propan-2-ol (Isopropanol)	Fisher Scientific GmbH, Schwerte, Germany
Recombinant Human/Murine/Rat Activin A (E. coli derived)	PeproTech Germany, Hamburg, Germany
RNASE AWAY®	Molecular BioProducts Inc., San Diego, CA, USA
Sodium azide (NaN_3)	Sigma-Aldrich, St. Louis, MO, USA
Sodium chloride (NaCl)	Carl Roth GmbH + Co. KG, Karlsruhe, Germany
Sodium dodecyl sulfate (SDS), ≥ 99%	AppliChem GmbH, Darmstadt, Germany
ß-Mercaptoethanol for molecular biology	AppliChem GmbH, Darmstadt, Germany
ß-Mercaptoethanol, suitable for cell culture	Sigma-Aldrich Co., St. Louis, MO, USA
Taurine	Sigma-Aldrich Co., St. Louis, MO, USA
Tris(hydroxymethyl)aminomethane (Tris)	Affymetrix, Santa Clara, CA, USA
Triton™ X-100	VWR International GmbH, Darmstadt, Germany

3.7 DNA Molecular Weight Marker

Table 10. Molecular weight marker used in the study.

Product	Company
Gene Ruler™ DNA Ladder Mix	Thermo Fisher Scientific, Waltham, MA, US

3.8 Cell Culture and Bacterial Media and Buffers

3.8.1 Cell Culture Media Components

Table 11. Components of cell culture media used in the study.

Product	Company
mTeSR™ Plus Basal Medium	STEMCELL Technologies Canada Inc., Vancouver, BC, Canada
mTeSR™ Plus 5X Supplement	STEMCELL Technologies Canada Inc., Vancouver, BC, Canada
Ham's F-12 Nutrient Mix (F-12)	Thermo Fisher Scientific, Waltham, MA, USA
Dulbecco's Modified Eagle Medium (DMEM)/F-12 (1:1) + GlutaMAX™ (1x)	Thermo Fisher Scientific, Waltham, MA, USA
DMEM/F-12 (1:1)	Thermo Fisher Scientific, Waltham, MA, USA
KnockOut™ DMEM	Thermo Fisher Scientific, Waltham, MA, USA
Fetal Bovine Serum, qualified, heat inactivated (FBS, HI)	Thermo Fisher Scientific, Waltham, MA, USA
KnockOut™ Serum Replacement	Thermo Fisher Scientific, Waltham, MA, USA
Minimum Essential Medium Non-Essential Amino Acids (100x) (NEAA)	Life Technologies Limited, Paisley, UK
GlutaMAX™ (100x)	Thermo Fisher Scientific, Waltham, MA, USA
L-Glutamine 200mM (100x)	Thermo Fisher Scientific, Waltham, MA, USA
Antibiotic-Antimycotic (100x)	Thermo Fisher Scientific, Waltham, MA, USA
N2 Supplement (100x)	Thermo Fisher Scientific, Waltham, MA, USA
B27™ Supplement (50x) without vitamin A	Thermo Fisher Scientific, Waltham, MA, USA
B27™ Supplement (50x)	Thermo Fisher Scientific, Waltham, MA, USA
Gentamicin solution (50 mg/ml)	Sigma-Aldrich Co., St. Louis, MO, USA

3.8.2 Cell Culture Media

All media were sterile filtered and used within 14 days. The sterile filtration was conducted with the vacuum filtration units listed among the consumables (section 3.12). The media were stored at 4°C and warmed to room temperature prior to use.

Table 12. Cell culture media used in the study.

Medium	Composition
mTeSR™ Plus	mTeSR™ Plus Basal Medium, 400 ml mTeSR™ Plus 5X Supplement, 100 ml For hiPSC culture: Gentamicin 25 µg/ml
Neural Induction Medium (NIM; white)	DMEM high glucose and F-12 on 1:1 ratio NEAA (100x) 1% GlutaMAX™ (100x) 1%

	N2 Supplement (100x) 1% Heparin sodium salt 2 µg/ml
Retinal Differentiation Medium (RDM; green)	DMEM high glucose and F-12 on 3:1 ratio B27™ Supplement (50x,) without vitamin A 2% NEAA (100x) 1% GlutaMAX™ (100x) 1% Antibiotic-Antimycotic (100x) 1%
RC2 medium (yellow)	DMEM high glucose and F-12 on 3:1 ratio FBS, HI 10% B27™ Supplement (50x) 2% NEAA (100x) 1% GlutaMAX™ (100x) 1% Antibiotic-Antimycotic (100x) 1% Taurine (100 mM) 0,1%
RC1 medium (red)	DMEM/F-12 (1:1) + GlutaMAX™ (1x) FBS, HI 10% N2 Supplement (100x) 1% NEAA (100x) 1% Antibiotic-Antimycotic (100x) 1% Taurine (100 mM) 0,1%
kRPE-medium	KnockOut™ DMEM Knockout serum replacement 20% NEAA (100x) 1% L-Glutamine 1% Gentamicin 0.05% ß-Mercaptoethanol 0.1 mM Nicotinamide 1.2 mg/ml Fourth and fifth differentiation weeks: Activin A 62 ng/ml

Table 13. Stocks of cell media supplements with solvents, concentrations, and storage temperature.

Supplement	Solvent	Concentration	Storage temperature
Blebbistatin	DMSO	10 µM	-80°C
BMP4	4 mM HCl + 0.1% Albumin from human serum	1.5 nM	-80°C
Heparin sodium salt	H_2O (Millipore)	20 mg/ml	-20°C
Taurine	H_2O (Millipore)	100 mM	-20°C
Retinoic acid	DMSO	10 mM	-80°C

3.8.3 Buffers

Table 14. Buffers used in the study.

Buffer	Composition/Company
Dulbecco's Phosphate Buffered Saline (DPBS) no calcium, no magnesium	Thermo Fisher Scientific, Waltham, MA, USA
CryoStor®CS10	STEMCELL Technologies Canada Inc., Vancouver, BC, Canada
Epredia™ Neg-50™ Frozen Section Medium	Fisher Scientific GmbH, Schwerte, Germany
Hepes (1M) Buffer solution	Thermo Fisher Scientific, Waltham, MA, USA
5x TBE	Tris 0.5 M Boric acid 0.5 M

	EDTA 10mM H_2O distilled
Laird's buffer	0.5 M Tris (pH 8) 25 ml 0.5 M EDTA (pH 8) 2.5 ml SDS 20% 2.5 ml 5 M NaCl 10 ml Millipore H_2O 210 ml
10x PBS	NaCl 80 g KCl 2 g $Na_2HPO_4 \cdot H_2O$ 14.4 g KH_2PO_4 2.4 g H_2O distilled 1 l

3.9 Consumables

Table 15. Consumables that were used for the cell culture.

Product	Company
24 well cell culture plate, sterile, with lid	Greiner Bio-One GmbH, Frickenhausen, Germany
25cm^2 Flask (rectangular canted neck, with vent cap, ultra-low-attachment surface)	Corning, NY, USA
6 well cell culture plate, sterile, with lid	Greiner Bio-One GmbH, Frickenhausen, Germany
8-lid chain, flat	SARSTEDT AG & Co. KG, Nümbrecht, Germany
96 well plate (ultra-low cluster, round bottom, ultra-low attachment)	Corning, NY, USA
BD Microlance™ Cannulas 27 G 3/4 0,4x19 mm	Becton Dickinson, Fraga, Spain
Bemis™ Parafilm™ M Laboratory Wrapping Film (PM-996)	Fisher Scientific GmbH, Schwerte, Germany
Cell scrapers, sterilized	TTP Techno Plastic Products AG, Trasadingen, Switzerland
Corning® 150 mL Vacuum Filter/Storage Bottle System, 0.22 µm Pore	Corning, NY, USA
Costar® 24 well plate (with lid, flat bottom, ultra-low-attachment surface)	Corning, NY, USA
Cover slips, round, 13 mm*	VWR International GmbH, Darmstadt, Germany
Disposable base molds, 7 x 7 x 5 mm	Ted Pella Inc., Redding, CA, USA
Disposable nitrile examination gloves, powder free	Paperlynen GmbH, Krailling, Germany
ep Dualfilter T.I.P.S® filter tips, 20 – 300 µl	Eppendorf AG, Hamburg, Germany
Filter tips 0 – 100 µl	nerbe plus GmbH & Co. KG, Winsen/Luhe, Germany
Filter tips 100 – 1250 µl	nerbe plus GmbH & Co. KG, Winsen/Luhe, Germany
Filter tips, super slim, 0.1 – 10 µl	nerbe plus GmbH & Co. KG, Winsen/Luhe, Germany
Filtropur V25, Vacuum filtration unit, 250 ml, PES, 0.2 µm	SARSTEDT AG & Co. KG, Nümbrecht, Germany
Filtropur V50, Vacuum filtration unit, 500 ml, PES, 0.2 µm	SARSTEDT AG & Co. KG, Nümbrecht, Germany
Micro tube 0.5 ml SafeSeal*	SARSTEDT AG & Co. KG, Nümbrecht, Germany

Micro tube 2.0 ml SafeSeal*	SARSTEDT AG & Co. KG, Nümbrecht, Germany
Multiply®-µStrip, 0,2 ml chain	SARSTEDT AG & Co. KG, Nümbrecht, Germany
Pipet 5 ml disposable, glass, serological, sterile	Corning, NY, USA
Pipette 10 ml, sterile, single packed	Greiner Bio-One GmbH, Frickenhausen, Germany
Pipette 25 ml, sterile, single packed	Greiner Bio-One GmbH, Frickenhausen, Germany
Pipette 50 ml, sterile, single packed	SARSTEDT AG & Co. KG, Nümbrecht, Germany
Pipette tips, 0.1 – 20 µl	nerbe plus GmbH & Co. KG, Winsen/Luhe, Germany
Pipette tips, 1 – 200 µl	VWR International, West Chester, PA, USA
Pipette tips, 100 – 1250 µl	nerbe plus GmbH & Co. KG, Winsen/Luhe, Germany
Reagent reservoir, 25 ml, disposable, pre-sterile	VWR International, West Chester, PA, USA
Safe-Lock Tubes 1.5 ml*	Eppendorf AG, Hamburg, Germany
Sterile 50 ml Disposable Vacuum Filtration System, 0.45 µm Durapore®	Merck KGaA, Darmstadt, Germany
SuperFrost®Plus Microscope slides	VWR International BVBA, Leuven, Belgium
Syringe 1 ml	Becton Dickinson S.A., Madrid, Spain
TC-dish, 100, standard	SARSTEDT AG & Co. KG, Nümbrecht, Germany
TC-plate, 6 well, standard	SARSTEDT AG & Co. KG, Nümbrecht, Germany
ThinCert™ 12 well plate, with lid, sterile	Greiner Bio-One GmbH, Frickenhausen, Germany
ThinCert™ Cell culture insert for 12 well plates, sterile, pore diameter: 0.4 µm	Greiner Bio-One GmbH, Frickenhausen, Germany
Tube, 15 ml, PP, conical bottom, CELLSTAR®, sterile	Greiner Bio-One GmbH, Frickenhausen, Germany
Tube, 50 ml, PP, conical bottom, CELLSTAR®, sterile	Greiner Bio-One GmbH, Frickenhausen, Germany
Weighing pan	VWR International GmbH, Darmstadt, Germany

*Products were autoclaved prior to usage for cell culture.

3.10 Devices

Table 16. Devices used in the study.

Device	Company
Autoclave Systec V-150	Systec GmbH, Wattenberg, Germany
Bio Vortex V1	Biosan, Riga, Lettland
BlueMarine 200 Electrophoresis chamber	SERVA Electrophoresis GmbH, Heidelberg, Germany
BluePower Plus Power supply unit	SERVA Electrophoresis GmbH, Heidelberg, Germany
Brady BMP61	Brady, Milwaukee, WI, USA
CASY® Cell counter and analyzer TT	Roche Innovatis AG, Reutlingen, Germany
Centrifuge 5415 R	Eppendorf AG, Hamburg, Germany
Centrifuge 5810	Eppendorf AG, Hamburg, Germany
Centrifuge Megafuge 1.0R	Heraeus Holding GmbH, Hanau, Germany
CO_2-Incubator Binder CB 160	Binder GmbH, Tuttlingen, Germany
CO_2-Incubator Binder CB 210	Binder GmbH, Tuttlingen, Germany

CO_2-Incubator Heraeus instruments	Heraeus Holding GmbH, Hanau, Germany
Compact shaker KS 15	Edmund Bühler GmbH, Bodelshausen, Germany
Eppendorf Research® plus pipet, 8-channel, variable, 30 – 300 µl	Eppendorf AG, Hamburg, Germany
Eppendorf Research® pipet, single-channel, 0.5 – 10 µl	Eppendorf AG, Hamburg, Germany
Eppendorf Research® pipet, single-channel, 10 - 100 µl	Eppendorf AG, Hamburg, Germany
Eppendorf Research® pipet, single-channel, 100 – 1000 µl	Eppendorf AG, Hamburg, Germany
Heraeus® Biofuge® pico	Kendro Laboratory Products, Osterode, Germany
Ice Maker Machine KBS	KBS Gastrotechnik GmbH, Wiesbaden, Germany
Incubator hood TH 15	Edmund Bühler GmbH, Bodelshausen, Germany
iPhone 12 mini	Apple Inc., Cupertino, CA, USA
J2-HS Centrifuge	Beckman Coulter Life Sciences, IN, USA
Leica KL 1500 LCD cold light source	Leica Microsystems GmbH, Wetzlar, Germany
Liquid Nitrogen Freezer 1520 ETERNE	tec-Lab GmbH Taunusstein, Idstein, Germany
Microscope Leica S6 D	Leica Microsystems GmbH, Wetzlar, Germany
Microscope Nikon Eclipse TE2000-S	Nikon Instruments Europe BV, Amstelveen, The Netherlands
Microscope Nikon Eclipse TS100	Nikon Instruments Europe BV, Amstelveen, The Netherlands
Microscope Olympus Fluoview FV3000	OLYMPUS EUROPA SE & CO. KG, Hamburg, Germany
Microwave oven Clatronic® MW 786	Clatronic International GmbH, Kempen, Germany
Milli-Q-Synthesis water purification system	Merck KGaA, Darmstadt, Germany
Mini-centrifuge for strips D-6015	neoLab Migge GmbH, Heidelberg, Germany
NanoDrop ND-1000 Spectrophotometer	NanoDrop, Wilmington, DE, USA
Pipette controller accu-jet® pro	BRAND GmbH + Co. KG, Wertheim, Germany
Precision Scales Explorer	OHAUS, Nänikon, Switzerland
Safety cabinet HeraSafe HS-18	Heraeus Holding GmbH, Hanau, Germany
Safety cabinet ScanLaf Mars Safety Class 2	LaboGene A/S, Allerød, DK
Scales Adventurer	OHAUS, Nänikon, Switzerland
Shaker Duomax 1030	Heidolph Instruments GmbH & CO. KG, Schwabach, Germany
Shaker KS-500	Janke & Kunkel GmbH & CO. KG, Staufen i. Br., Germany
Sterile bank HeraSafe HS-12	Heraeus Holding GmbH, Hanau, Germany
The belly dancer® orbital shaker	Merck KGaA, Darmstadt, Germany
Thermocycler peqSTAR 2x Gradient	VWR International GmbH, Darmstadt, Germany
Thermocycler T1 Plus	Biometra GmbH, Göttingen, Germany
Thermocycler T3	Biometra GmbH, Göttingen, Germany
Thermomixer compact	Eppendorf AG, Hamburg, Germany
Tissue Lyser II	Qiagen GmbH, Hilden, Germany
Transilluminator UST-30M-8R	BioView Ltd., Billerica, MA, USA
Vacuum pump MZ 2 C	Vacuubrand GmbH, Wertheim, Germany
Water bath W12	Labortechnik Medingen, Arnsdorf, Germany

3.11 Software

Table 17. Software used in the study.

Software	Company
CorelDRAW® 2019 version 21.3.0.755	Corel Corporation, Ottawa, Ontario, Canada
Chromas, version 2.6.4	Technelysium Pty Ltd, South Brisbane, Australia
ImageJ 1.53d	Wayne Rasband, National Institutes of Health, USA
Inkspace 1.0.2 (e86c8708, 2021-01-15)	Inkscape Project, 2020. Available from: https://inkscape.org
MS Office 2019	Microsoft, Redmond, WA, USA
NIS Elements BR 3	Laboratory Imaging, Nikon Instruments Europe BV, The Netherlands
Snap Gene 2.8.2	GSL Biotech LLC, San Diego, CA, USA

4 Methods

4.1 Cultivation of hiPSCs

4.1.1 Cryopreservation and Thawing of hiPSCs

Three hiPSC lines were used in this study (Table 1). Control lines 1 and 2 were reprogrammed from adult skin fibroblasts with lentiviral vectors. Control line 3 was reprogrammed from PBMC with episomal vectors. No donor had a history of retinal pathology. Two clones from each line (Table 1) were used. After reprogramming, all hiPSCs were cryopreserved. For cryopreservation, the hiPSCs were centrifuged at 1200rpm for 5 minutes, and the supernatant was removed. The cells were resuspended in CryoStor® CS10, and transferred to a freezer set to -80°C. After overnight freezing, the hiPSCs were transferred to a liquid nitrogen tank for long-term storage.

Before thawing, 6-well plates were coated with Matrigel. The Matrigel coating was performed by suspending Matrigel (the required volume is given by the manufacturer) in 25 ml of cold DMEM/F-12. 1 ml was distributed per well and supplemented with 1 ml of DMEM/F-12. The coated plates were stored at 4ºC for up to 7 days. Directly before seeding, the plate was incubated at room temperature for 1 hour or 37ºC for 30 minutes. All remaining liquid was removed and replaced with mTESR Plus with Gentamicin. The cryopreserved hiPSCs were thawed quickly at 37ºC and centrifuged at 1200rpm for 5 minutes. The supernatant was removed, and the cells were gently resuspended in mTESR Plus with Gentamicin. The cells were transferred to wells of a 6-well plate and cultivated in a humidity-controlled incubator, set to 37ºC and 5% CO_2.

4.1.2 hiPSC Culture and Passaging

HiPSCs were cultivated in mTeSR Plus medium with Gentamicin. The medium was replaced daily. Mycoplasma Removal Agent (1:100) was added to the medium during the first week in culture after thawing.

When the hiPSC reached 50-60% confluency, they were passaged at a 1:2 – 1:5 ratio. The passaging ratio was determined considering the cell confluency and their tendency to spontaneous differentiation. Differentiated cells were marked using an inverted microscope and mechanically removed before passaging. The cells were washed once with DMEM/F-12 and incubated with dispase for 5 minutes at 37ºC. The hiPSC colonies were inspected under a microscope to confirm the detachment of the colony borders. The hiPSCs were then gently

washed with DMEM/F-12 and resuspended in mTeSR Plus medium. Using a glass serologic pipette and a cell scraper, the hiPSC were gently detached from the surface of the well and transferred to a new well in a previously determined ratio.

4.1.3 Detection of Pluripotency Markers by ICC Staining

The pluripotency of control line 3 was confirmed by performing ICC staining with antibodies for three pluripotency markers. For ICC, hiPSCs were cultivated on Matrigel-coated autoclaved glass coverslips. One day after the hiPSC were seeded on the coverslips, they were washed with 1x PBS and fixed in 4% PFA for 10 minutes. The coverslips were washed three times with 1x PBS for 5 minutes per wash and incubated with a blocking buffer at room temperature for one hour (Table 18).

Table 18. Blocking Buffer Composition.

Component	Amount
H_2O (Millipore)	785 µl
Goat serum	100 µl
10x PBS	100 µl
20% Triton	15 µl

After one hour, the blocking buffer was replaced with the primary antibody solution (Table 19) and incubated overnight at 4°C. The dilutions of the primary antibodies are listed in Table 4. Coverslips incubated without primary antibodies served as a control.

Table 19. Primary antibody solution.

Component	Amount
H_2O (Millipore)	865 µl
Goat serum	25 µl
10x PBS	100 µl
20% Triton	5 µl

The following day, the primary antibody solution was removed, and the coverslips were washed three times with 1x PBS for 10 minutes. The coverslips were incubated in the secondary antibody solution for several hours at room temperature. The secondary antibody solution had the same composition as the one with primary antibodies, with a difference that DAPI (1:2000) and secondary antibodies (Table 5) were added. The coverslips were washed with 1x PBS for 5 minutes and mounted on microscope slides in one drop of Dako fluorescence mounting medium. The slides were dried overnight in the dark and imaged using the confocal microscope Olympus Fluoview FV3000.

4.2 RO and RPE Differentiation

4.2.1 RO Differentiation

The RO differentiation protocol was based on Zhong et al. (61), modified by the addition of Bone Morphogenic Protein-4 (BMP4) as per Capowski et al. (72). In this project, two clones from three hiPSC lines (Table 1) were differentiated to ROs in two to three differentiations. All differentiations were initiated consecutively.

The differentiation procedure was performed as follows. On day 0, three wells of 70-80% or four wells of 50% confluent hiPSC were washed with sterile filtered DPBS and incubated with dispase at 37°C for 15 minutes. Afterwards, the hiPSCs were washed twice with sterile, filtered DPBS and then mechanically dissociated. The cells were transferred to a 25mm^2 ultra-low attachment flask with 10 ml of mTeSR Plus medium supplemented with 10 µM blebbistatin. The medium was replaced on day 1 with a 3:1 ratio and on day 2 with a 1:1 ratio of mTeSR Plus medium and NIM (Table 12). On day 3, the medium was exchanged to 15 ml NIM. On day 6, the medium was replaced with 10 ml NIM, supplemented with 10 nM BMP4.

On day 7, the cell aggregates were transferred onto Matrigel-GFR-coated 6-well plates. The Matrigel-GFR coating was performed as in section 4.1.1 with the following modifications: 500 µl of Matrigel-GFR were solved in 14.5 ml of cold Knockout™ DMEM. Coated plates were incubated at 37°C for at least one hour before the cells were seeded. On day 9, 3 ml of NIM were added to each well, and on days 12 and 15, half was replaced with fresh NIM. On day 16, the medium was switched to RDM (Table 12). The medium and the cell culture plate were marked with a green sticker. The color-coded system was designed to decrease the likelihood of handling errors during the differentiation. Between days 18 and 24, the feeding medium was changed every other day.

Between days 22 and 24, neural domains were located with an inverted microscope and manually excised with two 27G needles on 1 ml syringes. Hepes (10 mM) was added to each well to equilibrate the pH. Detached ROs were transferred to separate wells of a U-bottomed 96-well plate with an ultra-low attachment surface. The adherent cells that had not formed neural domains were used for the byproduct RPE differentiation (section 4.2.2.1).

Half of the medium was replaced twice weekly during the fourth and fifth weeks of differentiation. In the sixth week, half of the medium was exchanged three times. On day 42, ROs were visually inspected under a microscope. ROs that had developed a bright outer rim were transferred to separate wells of a 24-well plate with an ultra-low attachment surface. From now on, the feeding medium was RC2 (Table 12). The medium and the cell culture plates were

marked with yellow stickers, as described previously. Hereafter, the ROs were cultured on the orbital shaker as per DiStefano et al. (75). Between days 42 and 62, the medium was exchanged twice per week.

During days 63 to 90, the medium was changed twice weekly with a 1 µM all-trans RA supplement. On three additional days, the RA was diluted with fresh medium and added to the ROs at a final concentration of 1µM. On day 91, ROs were visually inspected under a microscope, and those that had lost their bright outer rim were discarded. The remaining ROs were switched to RC1 medium supplemented with 0.5 µM RA. The medium and the cell culture plates were marked with red stickers. From this point on, the medium was exchanged twice weekly.

4.2.1.1 Fixation of ROs for Cryosections and ICC

ROs were fixated in 4% PFA at room temperature for 30 minutes. They were washed three times with 1x PBS for 5 minutes per wash and incubated with sucrose gradient at 4°C (6.75% and 12.5% for one hour, respectively, and 25% overnight). ROs were embedded in NEG-50™ medium on disposable base molds. They were stored at -80°C before cryosections. Cryosections were performed by Dr. Dr. Patricia Berber (PhD-student, Institute of Human Genetics) and Lisa Michaelis (former Parakenings; medical-technical assistant, Institute of Human Genetics).

4.2.1.2 ICC of ROs

Immunostainings of the cryosectioned ROs were performed by Dr. Dr. Patricia Berber. The cryosections on the microscopic slides were washed three times with 1x PBS for 5 minutes per wash and incubated with blocking solution (Table 18) at room temperature for one hour. The blocking solution was replaced with the primary antibody solution (Table 19). The slides were incubated at 4°C for 20-24 hours. The primary antibody solution was removed, and the slides were washed three times with 1x PBS for five minutes. The cryosections were incubated with the secondary antibody solution (Table 19) containing DAPI (1:2000) at room temperature for 2-4 hours. The slides were washed three times with 1x PBS for 5 minutes and covered in one drop of Dako fluorescence mounting medium with coverslips. The images were taken using the confocal microscope Olympus Fluoview FV3000 by Dr. Dr. Patricia Berber.

4.2.2 RPE Differentiation

4.2.2.1 Byproduct RPE Differentiation

Byproduct RPE (bRPE) differentiation branches off from RO differentiation in the fourth week. After ROs were excised from the 6-well plates, RDM was exchanged three times weekly. Several wells in each differentiation were randomly assigned to receive medium supplemented with nicotinamide (1.2 mg/mL). On day 42, the medium was replaced by RC2 medium. On day 48, half of the cells in each well were harvested for RNA isolation, as described in section 4.2.2.4. From the remaining half, clusters of pigmented cells were excised under an inverted microscope. The cells were dissociated with TrypLE at 37°C for 15 minutes, centrifugated at 1200 rpm for 4 minutes, and resuspended in the fresh medium. They were seeded on Matrigel-GFR coated 6-well plates. From this point on, the medium was changed twice a week. Treatment with nicotinamide was continued for selected wells. Around day 70 of differentiation, bRPE cells were passaged on new 6-well plates. Cells with a prominent cobblestone morphology were split 1:3 or 1:6, whereas cells without cobblestones were split 1:1. On day 91, the medium was switched to RC1 medium. Feeding intervals remained the same. Between day 100 and day 105, brightfield images were acquired from each differentiation under both conditions.

4.2.2.2 Krohne RPE Differentiation

The hiPSC control line 3 were also differentiated to RPE (kRPE) with alternative protocol as by (56). Three wells of 90-95% confluent hiPSC were used for each differentiation. On day 0, the mTeSR Plus medium was switched to kRPE medium (Table 12). The medium was changed daily. During the fourth and fifth weeks of differentiation, kRPE medium was supplemented with Activin A (62 ng/ml). In the seventh or eighth week, pigmented clusters of RPE cells were excised from the plate and passaged onto a 6-well plate with Matrigel-GFR-coating, as described in section 4.2. The medium was changed three times per week.

4.2.2.3 Passaging and Cryopreservation of RPE Cells

RPE cells were washed with sterile filtered DPBS and incubated with TrypLE at 37°C for 25 minutes. The cells were detached from the surface of the well through gentle pipetting and centrifuged at 1200 rpm for 4 minutes. The supernatant was discarded, and the cell pellet was resuspended in fresh medium, according to the split ratio, and transferred to a new Matrigel-CFR-coated 6-well plate or transwell filter inserts. Depending on their confluence, RPE cells were passaged on a 1:1, 1:3, or 1:6 ratio.

For cryopreservation, RPE cells were resuspended in CryoStor® CS10 and transferred to a freezer at -80°C. After being frozen overnight, they were stored in the liquid nitrogen tank.

4.2.2.4 Harvesting of kRPE, bRPE, and hiPSC for RNA Isolation

The cells were detached from the bottom of the wells and centrifugated. The supernatant was discarded, and the cells were resuspended in Lysis buffer and ß-Mercaptoethanol (1:100). A metal bead, cleaned in 3% H_2O_2 and DEPC H_2O, was added to the sample, and the cells were lysed on Tissue Lyser. The specimen was frozen on dry ice and stored at -80°C prior to RNA extraction.

4.2.2.5 qRT-PCR Analysis of hiPSC and bRPE

RNA isolation from harvested samples was performed with PureLink™ RNA mini kit by Lisa Michaelis. The RNA was then reverse transcribed to cDNA. The cDNA was amplified with gene-specific primers. The expression of 4 markers (BEST1, RPE65, MITF, and PMEL) was analyzed in three groups: hiPSCs and bRPE with and without nicotinamide supplementation. The results for bRPE were normalized against *Hypoxanthine Phosphoribosyltransferase 1* gene (a housekeeping gene) and expression levels in hiPSC. Afterwards, a normal distribution of the results in each group was verified with the Kolmogorov-Smirnov test. One-way ANOVA and Tukey-Kramer post hoc tests were performed to investigate the statistically significant difference (p-value < 0.05) between the three groups.

4.2.2.6 ICC of bRPE

The bRPE cells on the transwell filter inserts were fixed in 4% PFA for 10 minutes (30 minutes for cocultured bRPE). Afterwards, they were treated as described in section 4.1.3 with slight modifications. The bRPE cells were incubated with the secondary antibodies at 4°C for 20-24 hours. Finally, the filter inserts were mounted on the microscope slides with one drop of Dako mounting medium and covered with coverslips. The slides were dried overnight in the dark and imaged using the confocal microscope Olympus Fluoview FV3000.

4.3 RO-bRPE Coculture

4.3.1 BRPE-Aggregates

This experiment was conducted to determine whether bRPE cells could grow as aggregates in suspension. BRPE from each hiPSC line were detached from the surface of the

plate, centrifugated, and resuspended in a fresh medium. The bRPE cells from the hiPSC line 1 were grown in the presence of nicotinamide, while those from the hiPSC lines 2 and 3 were cultivated with RA. At the same time, blebbistatin, a compound shown to reduce apoptosis and enhance cell aggregation, was added to the medium (78).

The cell count in bRPE suspension was measured using the CASY® cell counter and analyzer. A previously determined number of bRPE cells (12.5, 25, 62.5, or 125 thousand) was seeded in three wells of a 96-well plate with a low attachment surface. After four days, the diameter of the aggregates was measured (Figure 8B) with the microscope. ICC was performed on the bPRE-aggregates from hiPSC lines 2 and 3.

4.3.2 RO Trimming

All ROs (including controls) were trimmed to the bright outer rim one week before the coculture induction. In this way, the undifferentiated parts could be removed. For this procedure, ROs were transferred to the 6-well plate with sterile PBS. They were trimmed with two 27G needles under the inverted microscope. Afterwards, the ROs were moved to a 24-well plate with an ultra-low attachment surface and received fresh RC1 medium.

4.3.3 RO-bRPE Coculture in Suspension

4.3.3.1 Static Coculture

On day 0, bRPE cells from hiPSC line 1 clone A were resuspended in RC1 medium containing 0.5 µM RA, following the standard passaging procedure in section 4.2.2.3. The cell count in bRPE suspension was measured using the CASY® cell counter and analyzer. The formula below determined the bRPE cell number needed to cover the RO surface. It relied on the diameter of bRPE aggregates (Figure 8B). The mean size of 3 bRPE aggregates from the hiPSC line 1 was found to be 563 µm for 25000 bRPE cells.

$$\frac{\mathbf{25000}\ \boldsymbol{bRPE\ cells}}{\mathbf{563}\ \mu\boldsymbol{m}} = \frac{\boldsymbol{x\ RPE\ cells}}{\boldsymbol{RO\ size}\ (\mu\boldsymbol{m})}$$

Formula 1. The calculation of the bRPE cell number depending on RO size. This formula was used to calculate the bRPE cell number for the RO-bRPE coculture. The diameter of all ROs (RO size) was measured before the coculture induction.

After counting the number of bRPE cells, the volume needed to contain a desired cell count for each RO was calculated. Just before introducing bRPE to the ROs, blebbistatin was added to the cell suspension.

All ROs received fresh RC1 medium with 10 µM blebbistatin and 0.5 µM RA. They were transferred to a 96-well plate with an ultra-low attachment surface. The bRPE cell suspension was carefully added to the ROs. Control ROs received 250 µl of the feeding medium without bRPE cells.

The coculture system was harvested for ICC after seven days. The harvesting and fixating process is described in section 4.2.1.1. The cocultured species were stained for photoreceptor (recoverin and rhodopsin) and RPE (BEST1 and RPE65) markers.

4.3.3.2 Coculture under Agitation

The coculture was induced with ROs and bRPE from the hiPSC line 2 clone A. The procedure was the same as the static coculture experiment but without adding blebbistatin to the cell medium. Furthermore, on day 1 and 2, half of the bRPE cells added to the ROs on day 0 was introduced to the coculture. The purpose of this modification was to improve the extent of bRPE coverage of the RO surface. The cocultured species and controls were harvested for immunofluorescence stainings after 14 days.

4.3.4 Adherent Coculture

The bRPE from the hiPSC line 1 clone A were passaged onto a 12-well plate with filter inserts. After four weeks, ROs from the same differentiation were placed onto the bRPE layer. ROs were not added to the control wells. 14 days later, the coculture system was harvested for the immunostainings. An attempt to fixate bRPE and ROs together failed, as ROs detached from the bRPE layer. So, ROs and bRPE were investigated separately. They were stained for ZO-1 and rhodopsin.

4.4 Identification of *RP1*-Knockout hiPSC Clones

4.4.1 Previous Work

This subproject aims to identify an *RP1*-knockout hiPSC clone that lacks both functional copies of the *RP1* gene. Dr. Dr. Patricia Berber designed 7 sgRNAs for the CRISPR/Cas9 system that targeted Exon 2 of the *RP1* gene in Benchling (69). Alexandra Tchiruchina (Bachelor student, Institute of Human Genetics) tested the efficiency of sgRNAs in fluorescence-based HEK-assay.

Dr. Dr. Patricia Berber and Nico Hertel (medical-technical assistant, Institute of Clinical Human Genetics) transfected hiPSC line 2 clone B with the four most efficient sgRNAs and Cas9 protein. Michelle Geigenfeind (6-weeks-intern, Institute of Human Genetics) sequenced

mixed clones of treated hiPSC and quantified the efficiencies of sgRNAs. gRNA KO_7 (Table 2) showed the best efficiency of 23.3%.

Nico Hertel dissociated the hiPSCs treated with the Cas9 protein and gRNA KO_7 to single cells. Most cells from the colonies were cryopreserved at -80°C. The leftover cells were harvested for genomic DNA extraction.

4.4.2 Genomic DNA Extraction from hiPSC

The hiPSCs were lysed with Laird's buffer and Pronase E for genomic DNA extraction. The DNA was separated from cell debris through centrifugation at 14000 rpm for 15 minutes, precipitated with 450 µl isopropanol, and washed with 500 µl 70% ethanol. Finally, the DNA was eluted in 50 µl H_2O (Millipore). The DNA concentration was measured with a NanoDrop ND-1000 spectrophotometer. The DNA samples were stored at -20°.

4.4.3 Amplification of Exon 2 of *RP1* Gene through PCR

PCR was performed on genomic DNA samples with RP1_Ex2.1_EcoR1_F and RP1_Ex2.2_BamHI_R primers (Table 3). The composition of the reaction mixture is shown in Table 20. For some samples, the reaction mixture with DMSO was used (Table 21). Thermocycler settings are listed in Table 22. The duration of the elongation step was calculated depending on the size of the PCR product: 1 min/1 kb.

Table 20. PCR reaction mixture.

Component	Amount
H_2O (Millipore)	15.9 µl
5X GoTaq® Reaction Buffer	5 µl
dNTPs	0.5 µl
Forward primer (10 µM)	0.8 µl
Reverse primer (10µM)	0.8 µl
GoTaq® Polymerase	0.1 µl
DNA template	2 µl

The amounts for one sample are shown.

Table 21. Reaction mixture for PCR with the use of DMSO.

Component	Amount
H_2O (Millipore)	14.7 µl
DMSO	1.3 µl
5X GoTaq® Reaction Buffer	5 µl
dNTPs	1 µl
Forward primer (10 µM)	0.5 µl
Reverse primer (10µM)	0.5 µl
GoTaq® Polymerase	0.1 µl
DNA template	2 µl

The amounts for one sample are shown.

Table 22. Thermocycler settings for PCR.

Reaction step	Temperature	Duration
1. Initial denaturation	94°C	4 min
2. Denaturation	94°C	30 sec
3. Annealing	58°C	30 sec
4. Elongation	72°C	50 sec
5. Final elongation	72°C	4 min
6. Pause	10°C	∞

Steps 2-4 were repeated 32-34 times, depending on the DNA concentration of the sample.

4.4.4 Agarose Gel Electrophoresis

The size of the PCR product was evaluated through agarose gel electrophoresis. TBE buffer was added to agarose powder (1.5% w/v) to make the gel. The solution was heated until it became a homogenous mixture and then cooled in ice water. Two drops of 0.07% ethidium bromide were added to the solution. The GeneRuler™ DNA Ladder mix served as a size standard. The PCR product was visualized under UV light.

4.4.5 Enzymatic PCR Cleanup

To prevent PCR primers and dNTPs from interfering with the primer for Sanger sequencing, the samples were treated with exonuclease I and antarctic phosphatase. The reaction mixture components are listed in Table 23. The reaction was incubated at 37°C and 80°C for 15 minutes.

Table 23. Reaction mixture for enzymatic PCR cleanup.

Component	Amount
H_2O (Millipore)	3.65 µl
Antarctic phosphatase	0.25 µl
Exonuclease I	0.1 µl
PCR product	1 µl

The amounts for one sample are shown.

4.4.6 Sanger Sequencing of PCR Product

DNA sequencing of cleaned PCR product was performed with BigDye® Terminator Cycle Sequencing Kit v3.1. The reaction mixture components are listed in Table 24. The RP1_Ex2.1_EcoR1_F primer was used in the reaction. Thermocycler settings are given in Table 25.

The DNA was precipitated with sodium azide and 100% ethanol and washed with 70% ethanol. It was then solved in Hi-Di™ Formamide. The sequencing was conducted in Abi3130x1 Genetic Analyzer. The results were evaluated in Chromas and SnapGene.

Table 24. Reaction mixture for Sanger sequencing.

Component	Amount
5x sequencing buffer	2 µl
Big Dye® Terminator	0.5 µl
Forward or Reverse primer (10µM)	1 µl
H_2O (Millipore)	1.5 µl
Cleanup sample	5 µl

The amounts for one sample are shown.

Table 25. Thermocycler settings for DNA sequencing.

Reaction step	Temperature	Duration
1. Initial denaturation	94°C	5 min
2. Denaturation	94°C	30 s
3. Annealing	55°C	30 s
4. Elongation	60°C	3 min
5. Final elongation	60°C	5 min
6. Pause	15°C	∞

Steps 2-4 were repeated 27 times.

5 Results

5.1 RO Differentiation

Two clones from three hiPSC lines were successfully differentiated to ROs using a previously established protocol adapted from Zhong et al. (61) and Capowski et al. (72). In this project, the differentiation procedure was adjusted to additionally generate RPE cells (termed byproduct RPE, abbreviated as bRPE) (Figure 5A). To fully evaluate the effectiveness of the modified protocol, each hiPSC clone underwent two to three separate differentiations, as listed in Figure 5C.

Previously, the pluripotency of hiPSC lines 1 and 2 was verified using RNA sequencing as per Müller et al. (79) (data not shown). In this thesis, the hiPSC line 3 was shown to express three pluripotency markers (hSSEA3, Tra1-60, and hNANOG) and the marker of proliferation Ki-67 (Ki67) (Figure 5B).

A

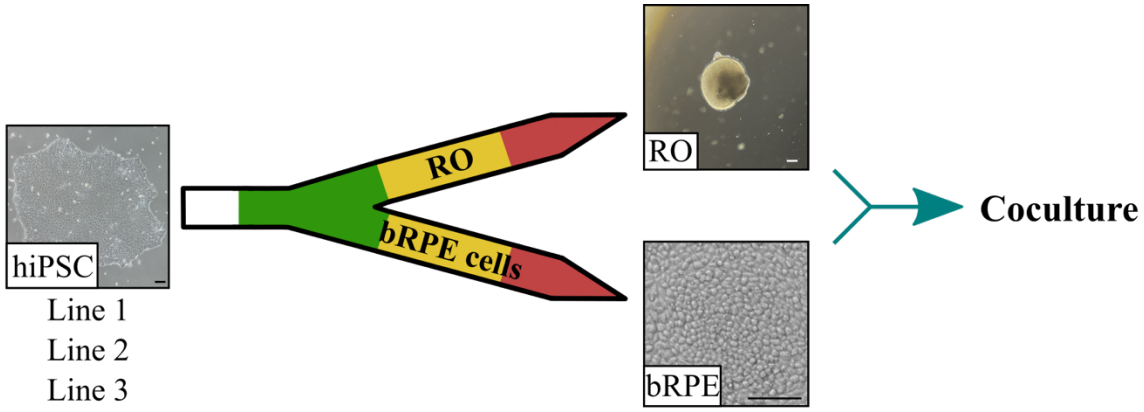

B

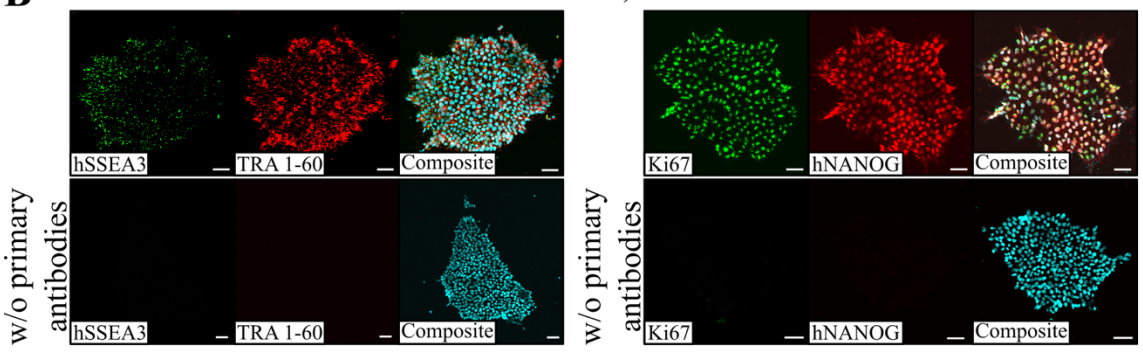

C

# of differentiations

	Clone A	Clone B
hiPSC line 1	3	2
hiPSC line 2	3	2
hiPSC line 3	2	2

Figure 5. RO and bRPE differentiation overview and hiPSC pluripotency. (A) The summary of RO and bRPE differentiation from hiPSCs is presented. The colors in the arrow denote the color-coded system of differentiation media. **(B)** The hiPSC line 3 was stained for three pluripotency markers (hNANOG, hSSEA3, and TRA 1-60) and a marker for cell proliferation (Ki67). The cells used for control purposes were not treated with primary antibodies. **(C)** The number of independent differentiations induced from each hiPSC clone is shown. Cell nuclei were counterstained with DAPI (B). Scale bars: 250 µm (A), 50 µm (B).

ROs were successfully acquired from every differentiation. In line with previous research, the number of obtained ROs varied among cell lines and differentiations (72,80). The yield of organoids from a single differentiation ranged from 1 to 29 after 63 days (Figure 6A). Despite the variable quantity, high-quality ROs identified via their characteristic bright outer rim were produced from every individual differentiation (Figure 6B) (61). The ROs were routinely screened, and those that lost their bright outer rim were discarded (Figure 6C).

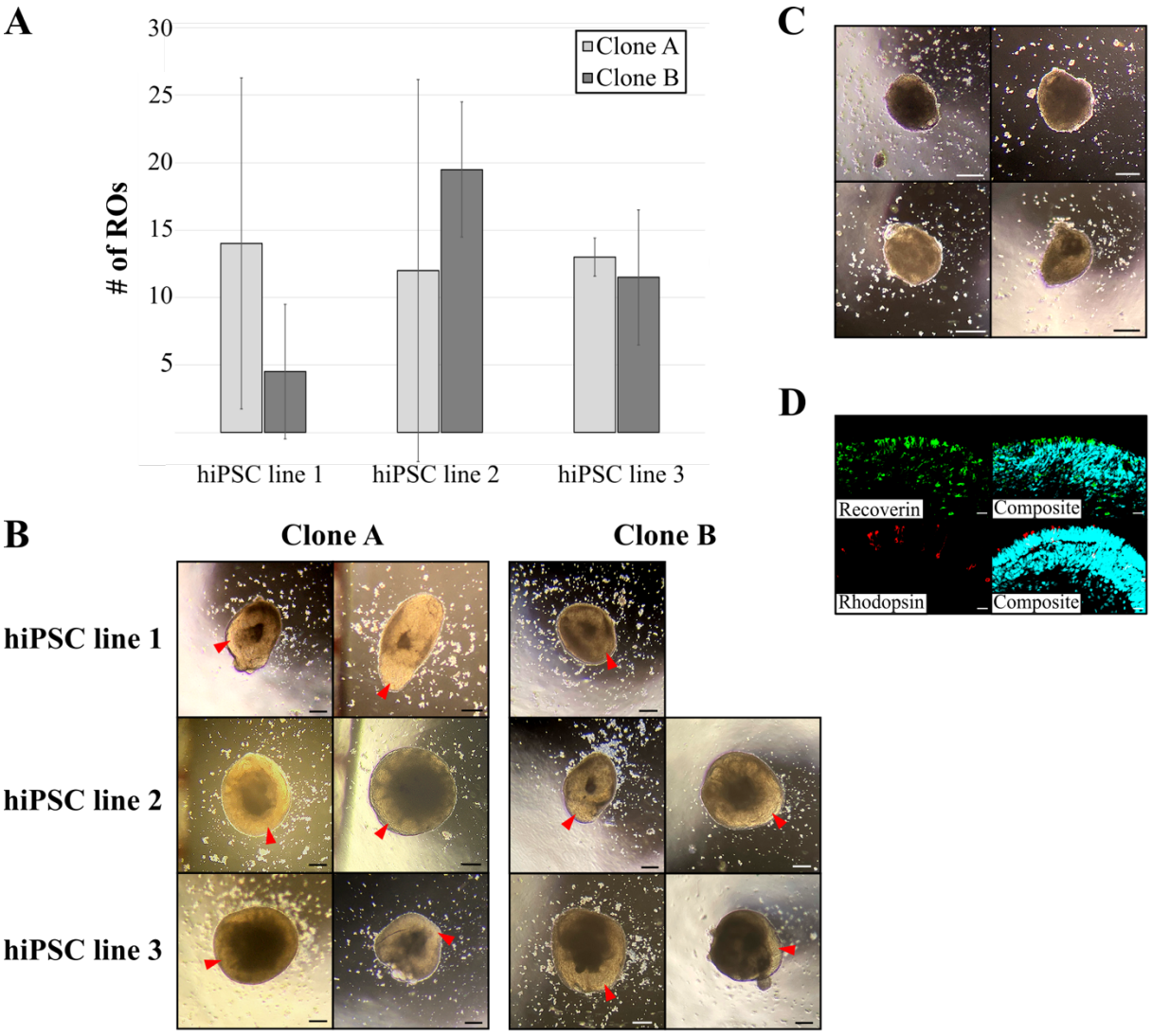

Figure 6. RO differentiation. (A) The number of high-quality ROs obtained from each hiPSC clone on differentiation day 63 is presented. Error bars denote the standard deviation. **(B)** On

differentiation day 42, the high-quality ROs with the characteristic bright outer rim (red arrowheads) were identified. **(C)** The low-quality ROs were discarded. **(D)** The high-quality ROs stained positive for two photoreceptor markers, recoverin and rhodopsin. Cell nuclei were counterstained with DAPI (D). Scale bar: 250 µm (B, C), 20 µm (D).

To assess photoreceptor development, cryosectioned ROs were immunostained for two markers: recoverin and rhodopsin. Recoverin is involved in the regulation of the phototransduction cascade. It is routinely used as a juvenile rod and cone photoreceptor marker (81), while rhodopsin is a mature rod marker (61,76,82). The expression of both proteins confirmed the presence of photoreceptors in the ROs (Figure 6D).

5.2 RPE Differentiation

Prior to this project, the hiPSCs that had not differentiated to ROs were discarded after the isolation of the developing organoids. The novel modification of the differentiation protocol was to cultivate these cells for three additional weeks. During this period, all differentiations produced clusters of pigmented cells, thought to be RPE. Half of the cells (pigmented and unpigmented) were harvested for qRT-PCR to evaluate the efficacy of the modified differentiation protocol.

The expression of four RPE markers in the bRPE cells was examined in comparison to the hiPSCs: microphthalmia-associated transcription factor (MITF), premelanosome protein (PMEL), Bestrophin-1 (BEST1), and retinal pigment epithelium-specific 65 kDa protein (RPE65) (Figure 7A). All markers have previously been used to characterize hiPSC-derived RPE (83,84). In this analysis, the expression of three markers increased significantly during the differentiation, while a tendency for higher RPE65 expression was shown ($p = 0.14$). Also, the effect of nicotinamide on the differentiating cells was investigated, as previous research demonstrated that this substance enhances RPE development *in vitro* (85). When comparing bRPE cells cultured with and without nicotinamide, it was found that the expression of MITF was significantly higher in the cells without nicotinamide supplementation.

To analyze the cell morphology, brightfield images of the bRPE from each differentiation were acquired (Figure 7B). The formation of cobblestones was evaluated since this is the typical morphology of highly confluent RPE cells (86). The cobblestones were observed in each bRPE differentiation exposed to nicotinamide. In contrast, the bRPE cells that did not receive this supplement only developed this characteristic appearance sporadically. Interestingly, the bRPE cells under the nicotinamide treatment could be split on a higher ratio than controls, thus leading to a greater RPE yield.

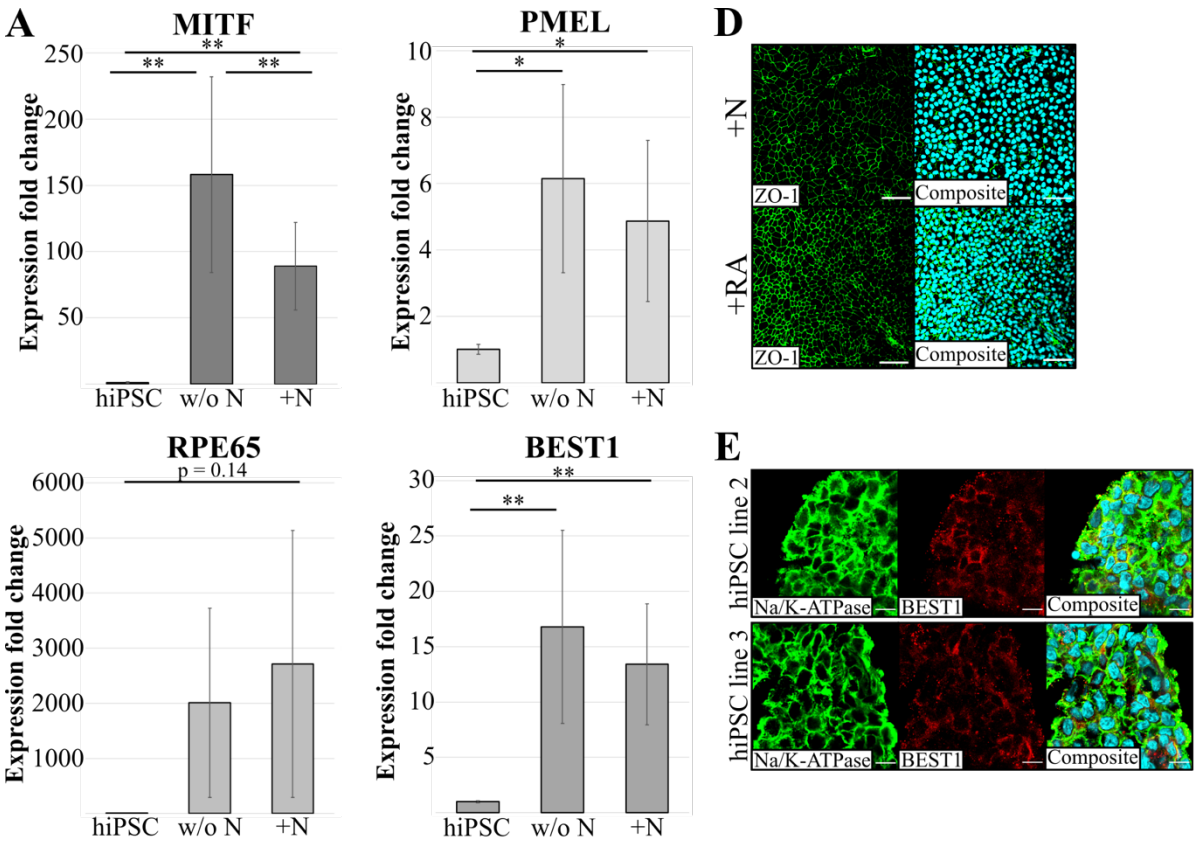
A
MITF
PMEL
RPE65
BEST1
Expression fold change
hiPSC
w/o N
+N
p = 0.14
D
+N
+RA
ZO-1
Composite
E
hiPSC line 2
hiPSC line 3
Na/K-ATPase
BEST1
Composite

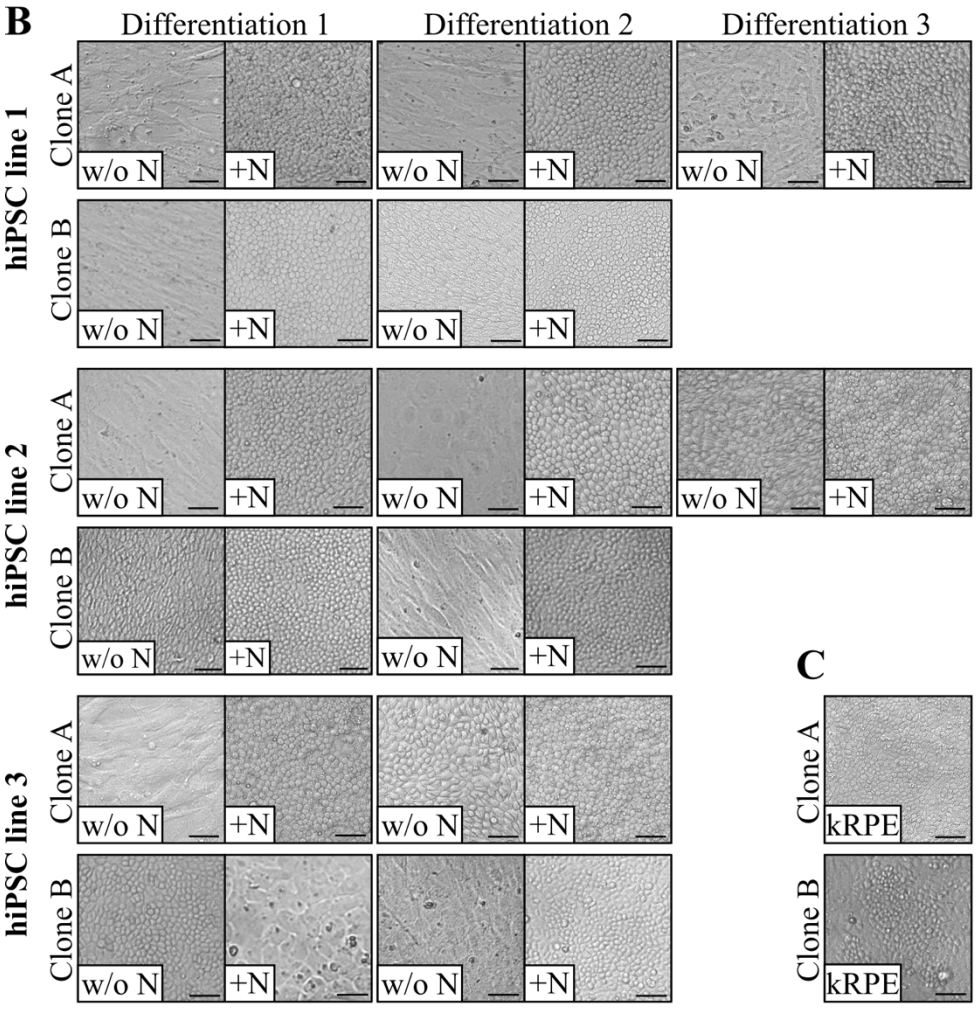
B
Differentiation 1
Differentiation 2
Differentiation 3
hiPSC line 1
hiPSC line 2
hiPSC line 3
Clone A
Clone B
w/o N
+N

C
Clone A
Clone B
kRPE

Figure 7. BRPE differentiation and characterization. (A) The expression of four RPE markers in the bRPE cells under (+N) and without nicotinamide treatment (w/o N) was analyzed via qRT-PCR. A significant increase in MITF, PMEL, and BEST1 expression was observed under both culture conditions. The error bars represent the standard deviation. *: $p < 0,05$; **: $p < 0,01$. **(B)** Brightfield images of the bRPE cells show the formation of cobblestones in all bRPE differentiations treated with nicotinamide (day 100-105). **(C)** Brightfield images of the kRPE cells from hiPSC line 3 confirm the cobblestone morphology. **(D)** The bRPE cells with nicotinamide (+N) and RA (+RA) supplementation were stained for ZO-1. **(E)** Immunofluorescent images of bRPE cells in suspension are presented. The cell nuclei were counterstained with DAPI (D, E). Scale bar: 50 µm (B, C, D), 10 µm (E).

Additionally, both clones from the hiPSC line 3 were differentiated to RPE (termed kRPE) as controls for our bRPE cells, using a previously established hiPSCs to RPE differentiation protocol (56,87). The cobblestone morphology of the kRPE cells was compared to the bRPE and found to be very similar (Figure 7C).

For further characterization of the bRPE cells, they were passaged onto transwell filter inserts previously shown to facilitate the polarization of RPE cells *in vitro* (87). After six weeks, we analyzed the bRPE via ICC (Figure 7D). The cells were immunostained for Zonula occludens-1 (ZO-1), a tight junction marker expressed in the cell membrane and used to assess RPE morphology *in vitro* (87). The analysis confirmed the distinctive hexagonal shape of the bRPE cells.

Overall, the bRPE cells were shown to be on par with RPE differentiated directly from hiPSCs, making them suitable for future experiments. Moreover, as previous research has verified that RPE retains its stability and functionality after being thawed, the cells from each hiPSC clone were cryopreserved for later research (87).

Two additional culturing conditions were tested on the bRPE in order to create the best possible starting point for future RO-RPE coculture experiments. The tolerance of the RO feeding medium was investigated in the bRPE. The cells were weaned off nicotinamide and switched to RA, a supplement of the RO medium. They were stained for ZO-1 to assess possible detrimental repercussions on the cell morphology. In this experiment, no adverse effects of RA were observed (Figure 7D).

Furthermore, we explored whether the bRPE cells could be grown in suspension, similar to ROs. For this experiment, bRPE cells from each hiPSC line were seeded on a 96-well plate with a low attachment surface. At the same time, blebbistatin, a compound shown to reduce apoptosis and enhance cell aggregation, was added to the medium (78). Under these conditions, the bRPE grew as cellular aggregates. After four days, the diameter of the aggregates was measured (Figure 8B). It was noticed that their size increased with the number of bRPE cells

seeded, though there was some variation among the cell lines. To further investigate the bRPE aggregates, the expression of BEST1 and Na^+/K^+-ATPase1 (Na^+/K^+-ATPase) was analyzed via immunofluorescent stainings (Figure 7E). The expression pattern of both markers was previously shown to reflect the characteristic morphology of RPE cells (83,87). Once again, there was no detectable negative impact on the bRPE due to culturing in suspension.

5.3 Investigating RO-RPE Coculture Conditions

It has been demonstrated before that the development of photoreceptors in ROs benefits from the interaction with RPE cells, as RPE is essential for photoreceptor functionality and survival *in vivo* (76,77). This study aimed to search for a simple and reproducible technique to coculture ROs and bRPE cells. Therefore, two conditions of suspension culture and one adherent coculture technique were investigated. All coculture experiments presented in this thesis are based on the rendezvous principle, where the ROs and bRPE from the same differentiation are reunited.

One week before the coculture induction, the ROs were trimmed to leave only the bright outer rim (Figure 8C), as previous studies have demonstrated that this morphology corresponds to the developing neural retina (61,72). The purpose of this method was to enhance the probability of attachment between photoreceptors and bRPE.

5.3.1 Static RO-bRPE Coculture in Suspension

An overview of the first coculture technique is presented in Figure 8A. The 105-day-old ROs and bRPE were used in this experiment. On the day of the coculture induction (day 0), six ROs were transferred to a 96-well plate with an ultra-low attachment surface (Figure 8D). Three ROs served as controls; to the other three, bRPE cells were added. The number of bRPE cells introduced to each organoid was determined to reflect its size (Formula 1). The calculations were based on the measured diameters of the bRPE aggregates (Figure 8B). Besides, blebbistatin was added to the cocultures and control ROs to facilitate the aggregation of the bRPE on the organoid surface.

The appearance of all ROs was monitored daily. The bRPE cells attached to the surface of each RO (day 1), although the number of adherent cells appeared to decrease over time (days 4 and 7) (Figure 8D). Furthermore, a prominent reduction in the clarity of the bright outer rim was observed in all six ROs.

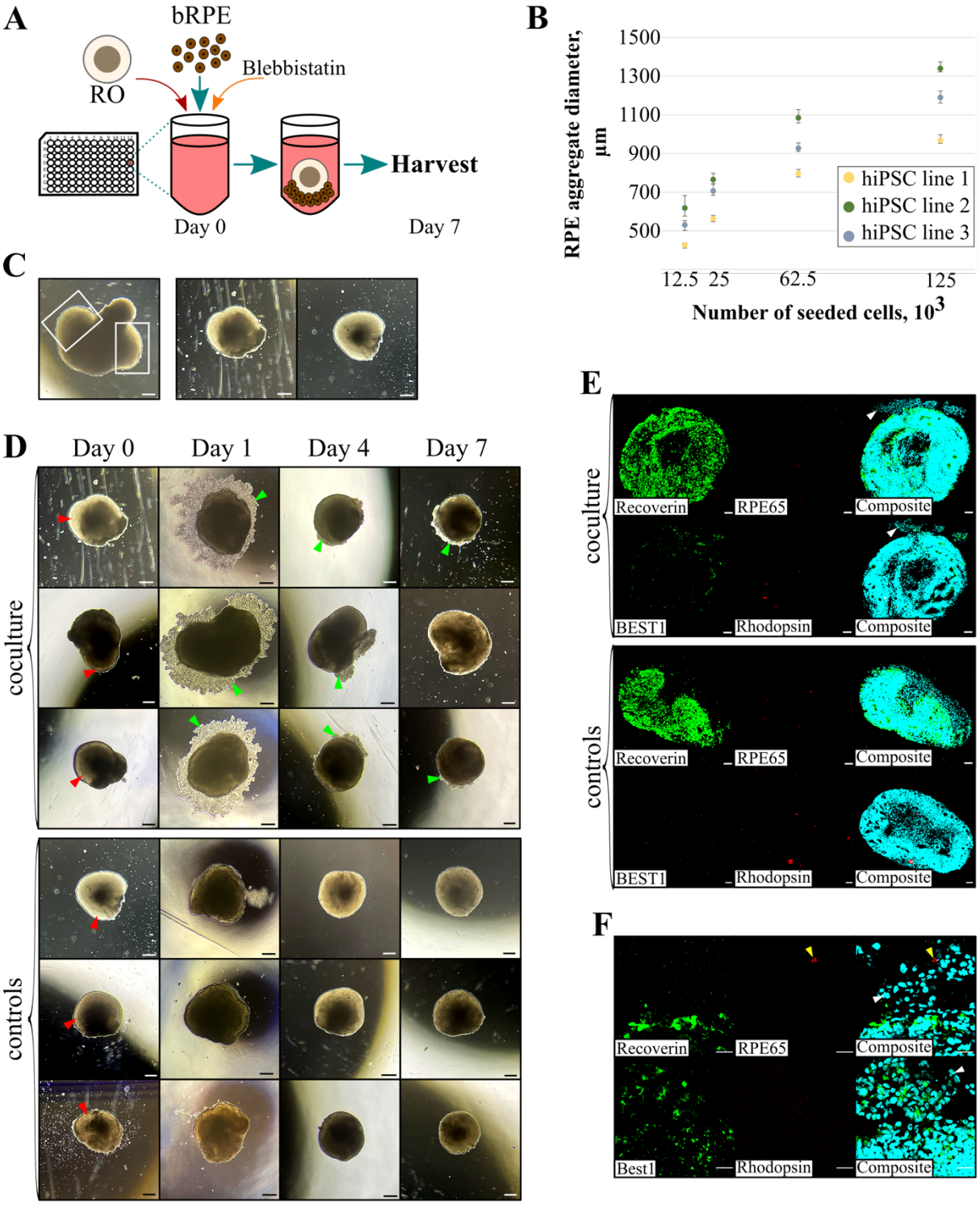

Figure 8. Static RO-bRPE coculture in suspension. (A) The schematic overview displays the course of the experiment. **(B)** An increase in the diameter of the bRPE aggregates with the number of seeded bRPE cells was observed. n = 3 aggregates per hiPSC line and cell number. **(C)** The ROs were trimmed before the coculture experiments. White rectangles denote the areas with the bright outer rim, which were excised and used for the coculture. **(D)** In the cell culture, the loss of the bright outer rim (red arrowheads) of all ROs and reduction in attached bRPE cells (green arrowheads) were observed. **(E)** The cocultured ROs and age-matched controls were stained for photoreceptor (recoverin and rhodopsin) and RPE (RPE65 and BEST1) markers. bRPE cells (white arrowheads) adhered to the RO and expressed BEST1. **(F)** The contact site of the cocultured ROs and bRPE is shown in a higher magnification. The bRPE

cells expressed BEST1 and RPE65 (yellow arrowheads). Cell nuclei were counterstained with DAPI (E, F). Scale bar: 250 µm (C, D), 50 µm (E), 20 µm (F).

After seven days, all ROs were harvested, cryosectioned, and immunostained for photoreceptor and RPE markers (Figure 8E-F). Two ROs cocultured with bRPE presented noticeable bRPE clusters in the immunofluorescent stainings (Figure 8E, white arrowheads). All ROs contained recoverin-positive photoreceptors, and a sporadic rhodopsin signal was detected. The bRPE cells expressed BEST1 and, infrequently, RPE65 (Figure 8F, yellow arrowheads). The preservation of the hexagonal morphology of bRPE was confirmed in the BEST1 staining.

5.3.2 RO-bRPE Coculture under Agitation

Figure 9A provides an overview of the second coculture experiment. The coculture was induced with four 105-day-old ROs and bRPE cells. We calculated the number of bRPE cells that would be introduced to the ROs as reported before (Formula 1). On days 1 and 2, half of the bRPE cells used on day 0 were added to the coculture. This time, the feeding medium was not supplemented with blebbistatin.

During the experiment, the control ROs showed no signs of losing their bright outer rim. The appearance of the cocultured ROs could be assessed only sporadically since they were occasionally covered by the bRPE cells (Figure 9B). A gradual reduction of the bRPE cells adherent to the ROs was noticed during the coculture. On day 14, all ROs were harvested for immunofluorescent stainings (Figure 9C). The images revealed that some bRPE cells remained attached to the ROs (Figure 9C, white arrowheads). Recoverin and rhodopsin expression in the ROs was also verified.

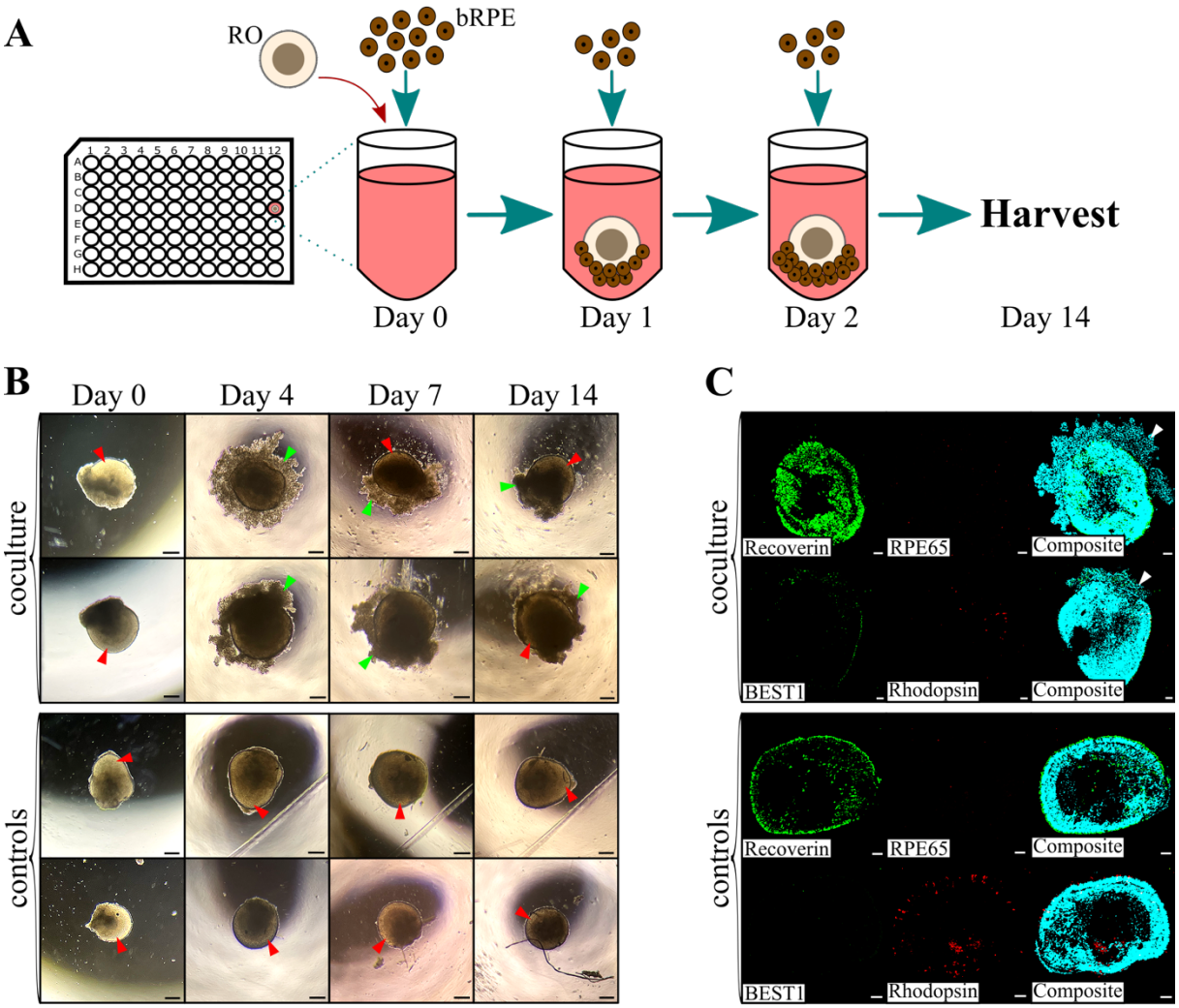

Figure 9. RO-bRPE coculture under agitation. (A) The scheme overviews the coculture experiment. **(B)** The bright outer rim (red arrowheads) of cocultured ROs and age-matched controls was observed in the cell culture until the harvest day. The gradual detachment of the bRPE cells (green arrowheads) from the ROs was noticed. **(C)** The ROs were stained with antibodies against photoreceptor (recoverin and rhodopsin) and RPE (RPE65 and BEST1) markers. The bRPE cells (white arrowheads) were shown to adhere to the ROs. Cell nuclei were counterstained with DAPI (C). Scale bar: 250 µm (B), 50 µm (C).

5.3.3 Adherent RO-bRPE Coculture

An overview of the third coculture technique is presented in Figure 10A. This experiment utilized 126-day-old ROs and bRPE cells. The bRPE cells were seeded onto transwell filter inserts four weeks prior to the coculture induction. On day 0, two ROs were placed on the bRPE layer. We used two ROs in suspension and two transwell filters with bRPE as controls.

As in the previous coculture experiments, the ROs were monitored regularly (Figure 10B). After three days, they seemed to adhere to the bRPE cells. This contact was

revealed as mechanically unstable, as one RO detached from the bRPE after a medium change. An appraisal of the bright outer rim could not be performed because the transwell filter inhibited the illumination of the RO under a microscope. After 14 days, the coculture systems were harvested. Both ROs detached from the bRPE during the harvest and were analyzed separately via ICC.

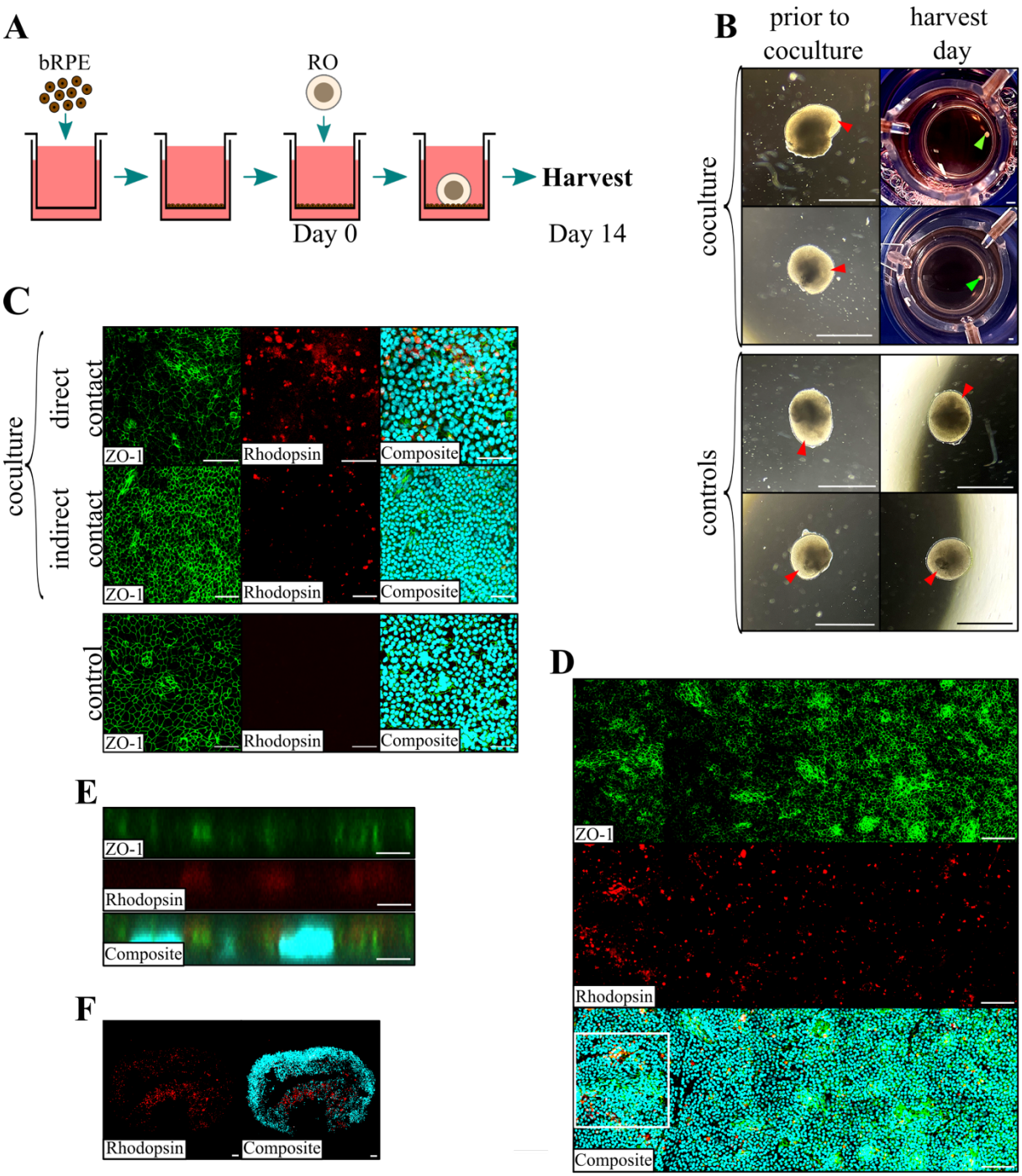

Figure 10. Adherent RO-bRPE coculture. (A) The sketch shows the adherent coculture experiment. **(B)** Images of the ROs on transwell filters with bRPE and control ROs are presented. Red arrowheads denote the bright outer rim of the ROs. Green arrowheads point to the ROs on the filter inserts. **(C)** Cocultured and control bRPE were stained for ZO-1 and

rhodopsin. The cocultured bRPE cells showed positive rhodopsin staining. **(D)** The image of a larger area of bRPE cells on the filter insert demonstrated a slight decrease in rhodopsin staining relative to the increasing distance from the RO position (white square). **(E)** An orthogonal view of a Z-stack confirmed the rhodopsin signal to be at the same level or below the ZO-1 staining, indicating uptake of rhodopsin by the bRPE. The apical side of the cells is projected to the top of the images. **(F)** The cocultured ROs stained positive for rhodopsin. Cell nuclei were counterstained with DAPI (C-F). Scale bars: 1 mm (B), 50 µm (C, F), 100 µm (D), 10 µm (E).

The bRPE cells were immunostained for ZO-1 and rhodopsin. The ZO-1 expression pattern confirmed the hexagonal morphology of the bRPE (Figure 10C). A prominent rhodopsin signal was observed in the bRPE cells that were in direct contact with the RO (Figure 10C). It decreased radially from the position of the RO, and even the bRPE cells furthest away stained positive for rhodopsin (Figure 10D). Z-stack images acquired at multiple positions confirmed the intracellular location of rhodopsin within the bRPE (Figure 10E). No rhodopsin signal was detected in the control bRPE cells (Figure 10C). Finally, the presence of rhodopsin-positive cells was confirmed in the cocultured ROs (Figure 10F). These findings indicate that the bRPE cells are capable of phagocyting rhodopsin-positive OSs.

5.4 Identification of *RP1*-Knockout hiPSC Clones

The objective of this subproject was to investigate DNA alterations in the hiPSCs previously treated with the CRISPR/Cas9 system. The sgRNA (Table 2) targeted exon 2 of the *RP1* gene (Figure 11A). It was speculated that induced DNA modifications may result in a homozygous frameshift mutation, leading to premature stop codons in both gene copies. If these stop codons lie before the final intron-exon border, mRNA transcribed from the mutated *RP1* gene will be degraded via nonsense-mediated decay, causing the lack of the RP1 protein in the cells (reviewed in(45)).

Subsequently to the CRISPR/Cas9 treatment, the hiPSCs were dissociated into 121 single clones (previous work at the institute). The genomic DNA of all hiPSC single clones was isolated, and a PCR reaction was performed to amplify exon 2 of the *RP1* gene. The PCR product from 32 hiPSC single clones was tested for insertions or deletions (indels). Within the single clones, 59.4% were not altered through CRISPR/Cas9 treatment and were categorized as wild type (Figure 11B). 37.5% contained a heterozygous indel, and one hiPSC single clone with a homozygous cytosine insertion (c.283_284insC) was identified. This mutation was predicted to lead to a premature stop codon within exon 2 of the *RP1* gene (p.Leu95Profs*39). According to the postulation introduced above, this hiPSC clone may exhibit the *RP1*-knockout phenotype.

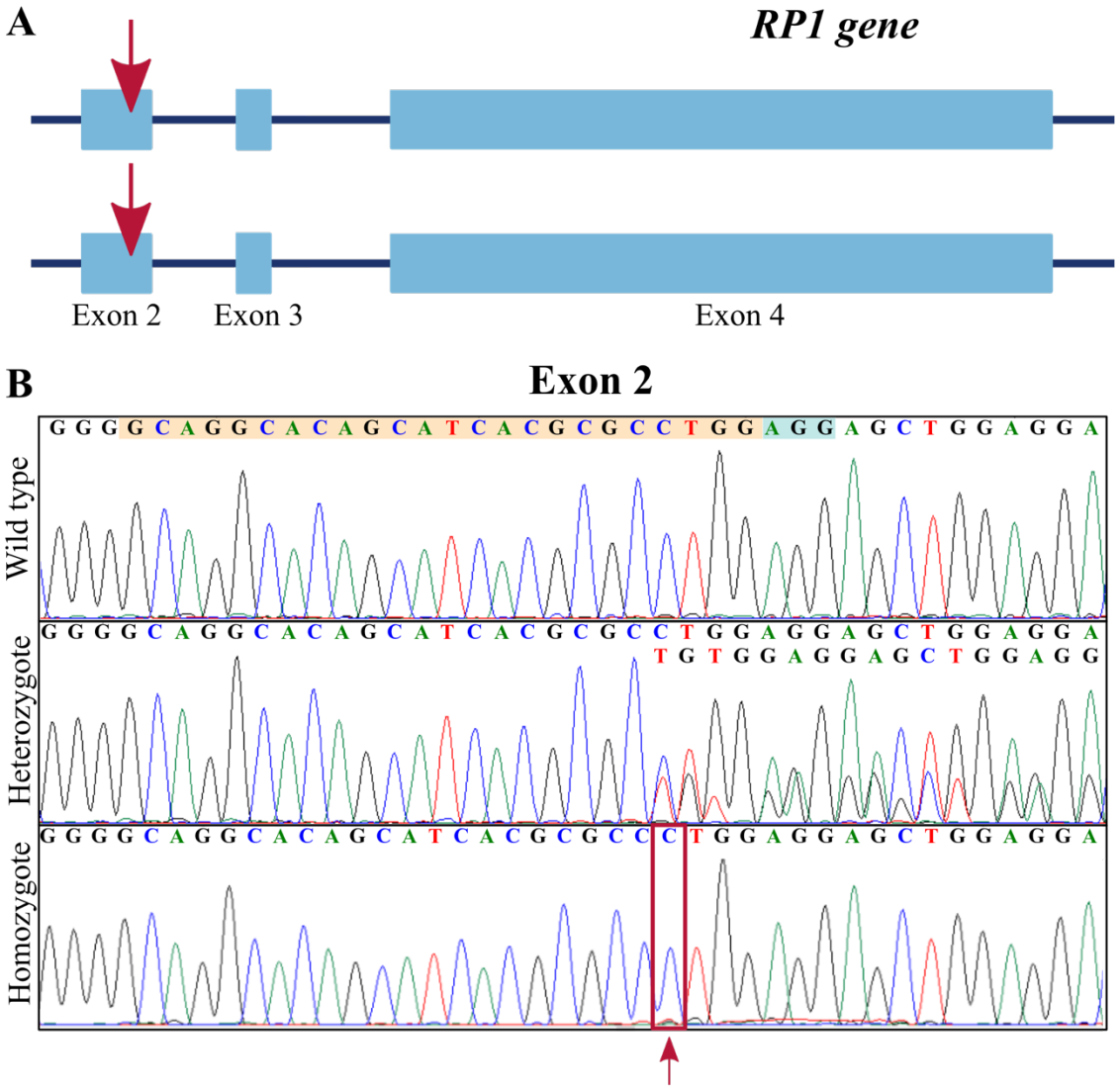

Figure 11. Identification of an RP1-knockout hiPSC clone. (A) A scheme of the *RP1* gene shows exons 2-4. The area targeted using the CRISPR/Cas9 system is indicated with arrows. **(B)** Exon 2 of the *RP1* gene was sequenced in 32 hiPSC single clones. Among them, hiPSC clones with no indels (wild type), heterozygous indels (heterozygotes), and one clone with a homozygous cytosine insertion (indicated in red) were found. The area where sgRNA bound is highlighted with beige. The protospacer adjacent motif (PAM) sequence is marked in blue.

6 Discussion

ROs are a highly sophisticated model system, which provides a unique opportunity to address diverse scientific questions concerning retinal development and disease. One advantage of ROs is that they contain multiple retinal cell types and, therefore, more closely mimic the *in vivo* cellular microenvironment than traditional monocultures (61). Nevertheless, there are also drawbacks to this cell culture system. A significant limitation of ROs is the absence of contact between photoreceptors and RPE monolayer (reviewed in (73)). *In vivo*, the RPE is an integral part of the photoreceptor support system. RPE cells perform multiple tasks to help maintain the physiological functions of the photoreceptors. They supply nutrients, phagocytose shed OS discs, and recycle photopigments needed for the phototransduction cascade (reviewed in (17)). In traditional ROs, photoreceptors are deprived of this crucial relationship with the RPE. Therefore, to date, utilizing ROs to study conditions affecting the photoreceptor-RPE system, including RP, is only feasible to a certain degree.

This study aimed to approach a possible solution to this problem. First, a reliable source of RPE cells must be available before physiological contact between the RPE and photoreceptors can be established *in vitro*. RO differentiations usually produce no or minimal amount of RPE cells. In this thesis, we have adapted the standard hiPSCs to ROs protocol to generate ROs and RPE cells, termed bRPE, simultaneously (Figure 5A). The differentiations of three hiPSC lines reliably resulted in high-quality ROs and pigmented bRPE cells. For mature bRPE, the expression of RPE-specific markers was verified via qRT-PCR and ICC (Figure 7A, 7D, 7E). Also, the hexagonal morphology of the bRPE was confirmed (Figure 7B). Finally, three techniques to coculture ROs and bRPE were investigated. In two experiments, ROs were cultured with bRPE in suspension (Figure 8 and 9). The third coculture was conducted under adherent conditions using the transwell filter inserts (Figure 10). The expression of photoreceptor and RPE markers was confirmed in the cocultured specimen. Moreover, the evidence indicating that the bRPE cells phagocytosed RO OSs was found in the adherent coculture.

The first crucial step towards RO-RPE coculture was successfully differentiating ROs from each hiPSC clone. As described in previous publications, the number of high-quality ROs varied greatly between hiPSC lines, clones, and differentiations (Figure 6A) (72,80). Potential sources of this inconsistency have long been discussed among researchers (reviewed in (88)). The genetic and epigenetic backgrounds of hiPSCs and their somatic progenitors have been considered possible factors impacting this variable differentiation capacity.

In 2011, Lister et al. assessed whole-genome DNA methylation at single-base resolution in independent hiPSC lines derived from female adipose-derived stem cells and lung fibroblasts (89). Their methylation status was compared to hESCs and somatic progenitor cells. The researchers found that 44-49% of differently methylated regions (DMRs) in hiPSCs, when compared to hESCs, reflected the methylation pattern of their somatic progenitor cells, indicating epigenetic memory. Thus, 51-56% of hiPSC-DMRs represented a de novo pattern neither detected in hESCs nor somatic progenitor cells. Finally, the research group showed that 88% of hypermethylated DMRs in hiPSCs were transmitted to the hiPSC-derived trophoblasts (89). The results of this study lead to the conclusion that the differences in the epigenetic status of hiPSCs and hESCs may be transferred to the differentiated cells and affect their gene expression.

Another study, conducted by Kim et al., compared DNA methylation of hiPSCs reprogrammed from umbilical cord blood cells (CB-hiPSCs) and neonatal keratinocytes (K-hiPSCs) (90). These progenitor cell types represent distinct germ layers: mesoderm and ectoderm, respectively. The CB-hiPSC and K-hiPSC lines also contained DMRs that reflected their somatic progenitor cell type. Both CB and K-hiPSCs were then differentiated to keratinocytes and hematopoietic cells. K-hiPSCs produced 23-fold more keratinocytes than CB-hiPSCs, while the reverse effect was observed for the hematopoietic colonies (90). These findings indicate that the progenitor cell type can influence the differentiation affinity of hiPSC lines and contribute to their capacity to produce certain cell types.

The influence of the epigenetic status of hiPSCs on retinal differentiation was explored by Wang et al. (91). Researchers reprogrammed five murine retinal cell types (rods and cones; amacrine/horizontal, bipolar, and Müller glia cells) into induced pluripotent stem cells (iPSCs) and analyzed their retinal differentiation capacity. The STEM-RET scoring system was used to evaluate the retinal differentiation (92). This study revealed that rods and bipolar cells showed the lowest reprogramming efficiency to iPSC. However, the iPSC lines originating from these cell types produced retinal tissue more frequently than other cell lines (91). IPSC epigenetic profiles indicated that rods and bipolar cells did not undergo the complete resetting of repressive epigenetic marks, and this memory impacted the subsequent differentiation of iPSCs. Also, the iPSC lines that effectively generated ROs were compared to those that failed to produce retina. Surprisingly, the iPSC lines with successful retinogenesis exhibited a more efficient resetting of retina-specific genes, promoters, and enhancers. The cruciality of stepwise activation of retina-specific genes during retinogenesis was suggested as a possible explanation for this remarkable phenomenon. This process was absent in iPSC lines with constantly activated genes

influencing retinogenesis. Based on these results, the authors conclude that epigenetic memory can positively or negatively impact the iPSC differentiation. Such exciting findings let us assume that further investigations into the epigenetic status of hiPSCs may lead to a more profound understanding of its impact on the differentiation protocol. Also, such results may allow researchers to predict the hiPSC differentiation capacity for a defined cell type.

Apart from the epigenetic status of the hiPSCs, the donor genetic background influences the fate of the future differentiations. Considering this, three cell lines chosen for this study were obtained from healthy individuals with no retinal or eye disorders history. Despite this thorough selection of the hiPSC donors, novel genetic alterations arising during the hiPSC culturing can affect subsequent differentiations (93,94).

In 2017, Kilpinen et al. compared copy number alterations (CNAs) between hiPSC lines and progenitor fibroblasts (93). 711 hiPSC lines from 301 healthy donors were obtained from the Human Induced Pluripotent Stem Cells Initiative. The analysis with genotyping arrays revealed that 41% of cell lines contained one or more CNAs, the three most frequent being a trisomy of the X-chromosome, chromosome 17 and 20. Further experiments showed a significant association of CNAs on chromosomes 17 and 20 with growth rate alterations of the hiPSCs (93). These results suggest the possible selection of hiPSCs with novel genetic mutations in the cell culture.

Another study analyzed the gene expression in 66 hiPSC lines, revealing that 20% carried chromosomal aberrations, while full trisomy was found in six cell lines (94). The higher passage of the hiPSCs seemed to be a risk factor for the chromosomal abnormalities. The researchers demonstrated that frequent trisomy or partial duplication of chromosome 12 led to the overexpression of the pluripotency genes *Nanog Homeobox* and *Growth Differentiation Factor 3*. The selection advantage of the cells with trisomy 12 was confirmed via qRT-PCR.

At this point, the hiPSC lines used in our study were not controlled regarding such alterations. Further investigations of the influence of CNAs on hiPSCs and their derivates may explain the heterogeneity of hiPSC culture and differentiation efficiency to some degree. With reference to all aspects mentioned above, one of the current challenges of hiPSC culturing is the absence of standardized protocols (reviewed in (95,96)). This makes hiPSC research prone to high inter-laboratory and inter-researcher variability. Only after developing uniform procedures and satisfactory quality controls, hiPSCs could be broadly applicable in regenerative medicine.

Previous research corroborates the effect of the hiPSC line not only on the number of ROs but also on their cellular composition (61,72,80). In 2014, Zhong et al. differentiated ROs

from three hiPSC lines and investigated the number and distribution of rhodopsin-positive cells after 21 weeks (61). They observed that two hiPSC lines produced ROs with strong rhodopsin signals, whereas organoids from the third hiPSC line contained rhodopsin-expressing cells only sporadically. Although this publication only examined the cells of the ROs, it is plausible that hiPSC lines with a higher intrinsic affinity towards a retinal fate produce more ROs per differentiation. In the future, the cellular composition of the ROs produced as a part of this project could be analyzed to investigate a possible correlation between the hiPSC lines that yielded a higher quantity of ROs in conjunction with their cellular organization.

Unfortunately, assessing the cellular composition of ROs is impossible on living organoids. For this reason, another method was chosen to monitor their well-being and development in the cell culture. In this project, the health of the ROs was judged by the presence of the bright outer rim (Figure 6B). Previous studies have indicated that this morphology corresponds to the developing neural retina. Therefore, it is often utilized as a parameter for quality control of the differentiation protocols (61,97). The benefit of doing this is that the bright outer rim can be appraised on the living organoid without the need to harvest it. In contrast, evaluating the RO cellular composition via ICC is undoubtedly a more accurate method to assess organoid quality but requires its harvesting.

Furthermore, research at this institute has revealed considerable variability among ROs, even those from the same differentiation (69). The consequence of this inter-organoid variability is that even if the high quality of one RO is confirmed via immunofluorescent stainings, other organoids from the same differentiation could still be substandard. We, therefore, chose to monitor the bright outer rim regularly and only sporadically investigated the cellular composition of the ROs. However, it should be noted that assessing the ROs' appearance can be challenging. ROs are 3D structures but can be inspected only from a single angle under the microscope. Thus, it is difficult to confidently judge the integrity of the bright outer rim at a specific moment. Moreover, distinguishing a healthy RO from one with a degraded outer rim is complex and requires extensive experience. Nevertheless, our method successfully generated photoreceptor-containing ROs suitable for the coculture experiments.

This study aimed not only to obtain healthy ROs but to simultaneously produce high-quality RPE cells, as traditional RO differentiations do not result in substantial quantities of RPE (reviewed in (73)). Our adapted protocol was applied to differentiate bRPE cells and ROs. With our adjustments, the bRPE cells were generated from each hiPSC clone. There are multiple advantages to our approach. Firstly, our modified procedure is a simple way to differentiate high-quality RPE cells with minimal extra time and resources. Also, ROs and

bRPE derive from the same pool of hiPSCs. The same genetic background and the same culture conditions for the first differentiation weeks for both tissues are significant benefits of this protocol. By these means, the influence of exogenous factors during cell culture was hoped to be reduced.

Besides, acquired ROs and bRPE are of the same age. So, using samples from the same differentiation for RO-bRPE coculture experiments would recapitulate their development *in vivo.* Nevertheless, it should be considered that pigmented clusters appeared 2 or 3 weeks after the emergence of ROs at week 4 of differentiation. This discrepancy could mean that the developmental stages of ROs and bRPE differ. However, due to the long maturation time of the ROs, a culturing time of months is expected for the RO-bRPE system. In this situation, a difference of several weeks in maturation would most likely have no impact. To further investigate the time point of bRPE emergence, the hiPSCs that had not produced organoids could be tested for RPE marker expression immediately after RO isolation. Maturing RPE cells, which are not yet pigmented, may already be present in culture.

In addition to testing our modified differentiation procedure, we examined the influence of nicotinamide on the developing bRPE. This vitamin has been reported to promote the hiPSC differentiation to RPE, and it is a standard component of the RPE feeding medium (85,87). Surprisingly, we did not observe a positive effect of nicotinamide on the expression of four RPE markers (Figure 7A). Instead, the expression of one of the pigment markers was significantly higher in the cells without nicotinamide addition. Therefore, we wondered whether the nicotinamide supplement was necessary to differentiate bRPE successfully. However, when the bRPE cells were passaged further, we noticed that bRPE treated with nicotinamide readily formed cobblestones, the typical morphology of RPE cells (86). In contrast, the cells without this substance in the medium only sporadically acquired this morphology. Furthermore, the cells under nicotinamide supplementation could be passaged in a higher ratio (1:3 or 1:6 with nicotinamide versus 1:1 or 1:2 without nicotinamide). Accordingly, the bRPE yield was notably greater from the differentiations treated with nicotinamide.

Based on these results, we theorize that nicotinamide is not essential for differentiating bRPE but enhances the expansion and maintenance of bRPE *in vitro*. If our hypothesis is confirmed, one could consider initiating the nicotinamide supplementation later when the RPE differentiation process has already been completed. Delaying the initiation of nicotinamide treatment may assist in developing a more robust bRPE population that can withstand nicotinamide withdrawal, should it be required for RO-bRPE cocultures, as our ROs have never been exposed to nicotinamide. Nevertheless, determining the optimal time for introducing

nicotinamide would take much work. Also, the positive effect of nicotinamide was cell-line dependent, so the most favorable time point would need to be established for each hiPSC line individually.

Typical RPE cell morphology and protein expression were confirmed in the bRPE (Figure 7D-E). Still, further experiments are needed to examine the functionality of bRPE cells in long-term cell culture. The RO-bRPE coculture must survive for a long time to study late-onset retinal diseases such as *RP1*-associated RP. The long-preserved bRPE are a requirement for such experiments. Further research at the institute confirmed the high quality of bRPE by evaluating their ability to phagocytize porcine photoreceptor OSs (98). The 168-day-old bRPE cells demonstrated the typical uptake and, after 4 hours, degradation of the OSs. *In vivo*, the phagocytosis of photoreceptor OSs is a critical task of RPE. Hence, the unimpaired function observed in the bRPE denotes their suitability for establishing cocultures with ROs.

After obtaining high-quality ROs and bRPE cells, the next step was to initiate the coculture experiments. Firstly, an optimal medium for the coculture had to be found. Both entities needed to be cultured in the same feeding medium without detrimental effects. Although the media for bRPE and ROs were broadly comparable, there were some noteworthy differences. The bRPE medium was supplemented with nicotinamide, while the RO medium contained RA. We considered ROs more sensitive than bRPE since they cannot be cryopreserved or expanded. Moreover, previous studies have shown that RA enhances photoreceptor development in ROs (61,74). As the final aim of the RO-bRPE coculture is to improve photoreceptor maturation, we were reluctant to deprive ROs of this supplement. Therefore, it was chosen not to alter the RO medium but to investigate whether the bRPE cells tolerate the removal of nicotinamide and exposure to RA.

It is yet possible that ROs can survive in the bRPE medium with nicotinamide. Previously, Shen et al. showed that nicotinamide improved the survival rate of neural cells due to a neuroprotective effect against oxygen and glucose deficiency (99). In their study, rat cortical neurons released significantly less lactate dehydrogenase when exposed to hypoxic conditions in the presence of nicotinamide. Additionally, the cell viability was improved.

Conversely, Regent et al. investigated the influence of nicotinamide on the RO yield and revealed that it increased the production of ROs from several hiPSC lines (100). However, if treated from the differentiation day 1 to 20, one hiPSC line showed substantially reduced RO yield. The authors, therefore, concluded that nicotinamide may have some adverse effects on the RO differentiation and shortened the exposure time to eight days. Under these conditions, all tested hiPSC lines produced significantly more ROs than controls. These findings, however

interesting for the early development of ROs, corroborate our decision not to expose our ROs to nicotinamide, as it could have had a detrimental impact at the late point in the differentiation. Before coculturing ROs and bRPE in a medium with nicotinamide, one should investigate whether ROs indeed tolerate nicotinamide for a long time, for example, by performing immunostainings for apoptosis markers.

Consequently, we explored whether bRPE cells can withstand nicotinamide deprivation and the addition of RA. Fortunately, there was no indication of an adverse effect of the RO medium on bRPE, as the expression and correct localization of BEST1 and ZO-1 in the bRPE exposed to RA were confirmed via ICC (Figure 7D-E). Nevertheless, it would be prudent to investigate the impact of the RO medium on bRPE more extensively. For example, it would be worthwhile to examine the ability of bRPE to phagocytose photoreceptor OSs in the bRPE medium versus the RO medium.

There is a possibility that bRPE cells perform better in the RO medium. Previously, it was reported that RPE cultures benefit from RA supplementation. Campochiaro et al. investigated the influence of RA on the RPE *in vitro* by evaluating cell growth and morphology (101). They found that RA successfully inhibited the overlapping growth of RPE, and the cells formed a monolayer. The assessment of growth curves revealed that RA supplementation resulted in significantly fewer cell numbers in culture. The authors hypothesized that RA inhibits RPE proliferation in a density-dependent manner. *In vivo*, RPE cells are constantly exposed to retinoids to which RA belongs, as their recycling is an integral part of visual transduction. *In vitro*, RPE cells are depleted of these substances, and RA supplementation may bring RPE maintenance in cell culture closer to the *in vivo* state. Nevertheless, as stated earlier, we observed that nicotinamide improved the passaging and growth rate of bRPE. Therefore, it was chosen to remove nicotinamide from bRPE cultures directly before the coculture induction.

In this study, the decision was made to test two types of RO-RPE coculture models: the adherent coculture and the coculture in suspension, since these are the conventional ways of culturing RPE and ROs, respectively. The suspension coculture technique had the advantage of keeping ROs closer to their regular culture conditions. However, these conditions may adversely affect the bRPE since RPE cells are typically grown in a different manner. Therefore, we conducted preliminary experiments and examined bRPE culture in suspension. BRPE cells from three hiPSC lines were seeded on an ultra-low attachment plate, and bRPE aggregates appeared in each well. The immunostaining confirmed the preservation of hexagonal cell morphology in these aggregates (Figure 7E). In the future, more extensive experiments can be

conducted to study the well-being of bRPE in suspension culture. For instance, the phagocytosis of OSs could be evaluated, or the expression of cell distress markers could be examined.

An earlier paper investigated the adherent coculture of ROs with murine RPE (76). RPE cells were plated on 6-well plates, and ROs were introduced once an RPE monolayer had formed. In the published report, RO death was observed in the coculture, most likely due to insufficient nutrient supply to the ROs. Therefore, the researchers cut their ROs into several pieces before coculturing. In our experiments, we also trimmed our ROs one week before the coculture induction to include only the bright outer rim (Figure 8C). This had several advantages. First, the ROs were smaller, facilitating the diffusion of fresh medium, which needed to be changed less frequently since the smaller ROs require fewer nutrients. Moreover, we hypothesized that removing the less developed areas of the ROs and focusing solely on the neural retina would increase the likelihood of contact between bRPE and photoreceptors. There were some risks to trimming the ROs, such as damage to the neural retina or bacterial or mycotic contamination. Nevertheless, we concluded that the benefits outweighed the stakes in this instance.

As no previous publications reported culturing ROs with RPE in suspension, establishing permanent contact between them in this setting was uncertain. Therefore, we searched for ways to enhance the RO-bRPE interaction. Earlier reports suggest that blebbistatin improves cell survival by reducing apoptotic bleb formation (78,102). Initially, blebbistatin was added to the bRPE aggregates, and no unfavorable effect on the cells was detected. Since blebbistatin was already part of our RO differentiation protocol, we assumed that reintroducing it to the ROs would be relatively safe. Surprisingly, the deterioration of the RO health after exposure to blebbistatin was observed during the static coculture in suspension (Figure 8D). So far, there have been no previous reports about the detrimental effects of blebbistatin on differentiated tissues such as ROs. Ultimately, we chose not to use blebbistatin in other cocultures. Using similar compounds was considered, but again, their influence on the ROs would be unpredictable. In the second suspension coculture technique, we investigated whether contact between ROs and bRPE could be established without additives. We observed that bRPE adhered to the RO and each other. Over time, some bRPE that had initially attached to the surface of the RO were lost.

The static coculture experiment detected that the bRPE cells were attached to only one side of the ROs (Figure 8D). So, in the suspension coculture under agitation, the bRPE were added to the coculture at three time points. We theorized that this would allow bRPE to cover the entire RO surface, as it was likely that ROs would rotate during the medium changes.

Unfortunately, after two weeks, it was noticed that the bRPE, which had covered much of the RO surface on day 4, remained attached only to a small area of the RO (Figure 9B). The disadvantage of the uneven bRPE distribution is that only some photoreceptors had direct contact with the bRPE. It is still possible for the photoreceptors without direct contact with bRPE to benefit from coculture. Some research groups have reported that photoreceptors had an enhanced light response after being treated with extracellular matrix-derived peptides from bovine RPE (103).

It should be noted, however, that other scientists fed ROs with RPE-conditioned media and did not observe an improvement in photoreceptor maturation (76). Furthermore, research groups that investigated photoreceptors in the ROs with RPE clumps also did not report a significant advancement in photoreceptor development (60,61). The RPE clusters may have been too small and contained too few cells to induce a noticeable effect on RO photoreceptors. Another plausible explanation is that soluble RPE factors cannot completely compensate for the absence of physical contact between photoreceptors and RPE. In contrast, this study aimed to investigate coculture techniques that introduce a physiological connection between ROs and RPE. Regrettably, no strong bond was observed in the suspension coculture, and the gradual reduction of the bRPE adherent to the ROs was evident.

In vivo, RPE cells are polarized and develop microvilli that enhance the RPE adhesion on photoreceptors (24). We must assume that the bRPE cells used in suspension cocultures were not polarized because they were cultured on a 6-well plate before the coculture induction. Previous reports have indicated that hiPSC-derived RPE cells grown this way reach lower polarization levels than those cultured on transwell filter inserts (87). In living organisms, however, RPE cells begin polarizing after contact with the photoreceptors is established (reviewed in (17)). In our suspension cocultures, the presence of photoreceptors could have induced the polarization of the bRPE. Whether two weeks of coculturing were sufficient to trigger this process remains to be determined. Suitable assays for investigating this issue could include examining apical and basal vascular endothelial growth factor secretion, which shows a higher apical release if the cells are polarized (87). However, it would be challenging to separate two compartments if bRPE cells were cultured in suspension. Alternatively, the localization of ZO-1 and BEST1 could be analyzed, as the former is expressed in the apical and the latter in the basolateral cell membrane sections. Furthermore, the formation of apical microvilli could be investigated via electron microscopy. If the hypothesis is confirmed that bRPE cells do not polarize in the suspension coculture, it may explain the poor bRPE adhesion on ROs.

The third coculture experiment was conducted under adherent conditions (Figure 10A). In contrast to the coculture in suspension, the bRPE were cultured on the transwell filter inserts before the RO introduction. A previous study showed that RPE cells cultured in this manner polarized and formed microvilli on the apical surface (87). We theorized that in this experiment, the interaction between photoreceptors and the bRPE would be facilitated, thereby creating a mechanically stable and intimate interaction. Unfortunately, this was not the case, and ROs detached from the bRPE during the harvest. Most likely, the photoreceptors separated from the bRPE at their most fragile segment, the connecting cilium. Since it would be exciting to analyze the interaction site between the RO and bRPE, some modifications of the adherent coculture technique would be required to prevent RO detachment in future experiments.

There are several possible ways to optimize the RO-bRPE connection in both coculture methods. One alternative could be to form a robust bRPE aggregate before inducing the coculture in suspension. In our experiments, the bRPE, supplemented with blebbistatin, formed aggregates after only a few days. The blebbistatin residue could be removed from the bRPE through successive medium changes, after which ROs could be safely introduced to the coculture. The advantage of this technique is that the bRPE aggregate would only have to establish contact with the RO.

Using a hydrogel is another method to stabilize the connection between RO and bRPE. A hydrogel is a network of crosslinked polymers that can provide a 3D scaffold for cells *in vitro*. A previous study used a hydrogel in their RO-RPE coculture, implying that it may provide mechanical stability (77). Still, if too much hydrogel is used, it may impede the nutrient supply to ROs. The hydrogel volume should be enough to stabilize the RO-bRPE contact but not lead to the undernourishment of the cells. In the best case, the bRPE would pass nutrients from the media to the RO in a regulated manner, thereby recapitulating the *in vivo* nutrient supply.

Further research at the institute utilized the bRPE cells mixed with Matrigel (a solubilized basement membrane extraction) for the coculture in suspension (98). At first, it was observed that the bRPE were distributed evenly around the RO and took up recoverin, a protein known to be expressed in developing photoreceptors. However, the distance between photoreceptors and bRPE increased after seven days in culture. It was also noted that the internalization of recoverin came to a standstill. These results suggest a temporary functional relationship between photoreceptors and bRPE in suspension. Surprisingly, in our adherent coculture, the bRPE cells were observed to phagocytose OS fragments without direct contact with the RO (Figure 10C-D). After seven days in suspension, ROs and bRPE were 90 µm apart (99). However, rhodopsin-positive bRPE cells were several hundred micrometers from the RO

in the culture on transwell filters. Considering this, the gap measured in coculture with Matrigel cannot explain the cessation of the recoverin uptake through bRPE. The discrepancy between the two coculture methods may be due to bRPE cells experiencing distress when cultured in suspension, reducing their ability to phagocytose OS fragments. Therefore, further experiments to closely monitor the well-being of bRPE are highly recommended if the coculture in suspension is to be pursued further. Nevertheless, the discovery of the functional RO-bRPE relationship under adherent conditions is a promising result for the feasibility of the RO-RPE coculture system. An exciting follow-up experiment would be an attempt to identify OS fragments in the bRPE via electron microscopy.

In contrast to our experiments, several research groups have explored an alternative RO-RPE coculture technique: coculture on microfluidic chips with vasculature-like perfusion. In 2019, Achberger et al. were the first to present the retina-on-a-chip method and reported the enhanced formation of OSs and the uptake of OS discs through the RPE in the coculture (77).

A recent study used a microfluidic chip to cultivate ROs and RPE derived from an RP patient with mutations in the *USH2A* gene (104). The USH2A protein, also known as usherin, is crucial for preserving photoreceptors and is associated with the basement membrane and ECM (105,106). Researchers differentiated RPE cells directly from the hiPSCs and seeded them onto 3D-printed, Matrigel-covered cell chambers (104). After two days, 18-day-old ROs coated with Matrigel were introduced to the coculture and left for 30 days on the chip. In the traditional culture, increased apoptosis, disorganization of ECM, and reduced expression of ECM components (laminin and collagen IV) were observed in patient ROs compared to controls. In contrast, the RO-RPE coculture seemed to mitigate the *USH2A* phenotype, as a significant increase of laminin- and collagen IV-positive areas was noticed in the cocultured organoids. Moreover, the improved overall survival of the ROs and the enhancement of RPE pigmentation were associated with culturing on the perfused chips. Therefore, the authors suggest that RO-RPE coculture on the microfluidic chip facilitates the *in vitro* development of ROs and RPE with *USH2A* mutations.

Unfortunately, the analysis of the RO-RPE interaction was not a subject of interest in this new study. Continuous perfusion with cell medium protects ROs from shearing forces during medium changes. It would be fascinating to investigate if abandonment of repeated feedings would stabilize the RO-RPE connection. Overall, microfluidic chips are a promising field of RO research that is attracting widespread interest from researchers. Creating a confined environment with a consistent supply of cell medium brings RO culturing closer to the

conditions found in living organisms. However, additional research is needed to investigate the growth of ROs on microfluidic chips over extended time.

Taking into account the long maturation time required for ROs, the RO-RPE cocultures must survive for an extended period. ROs have been cultured for up to two years, but long-term coculture with RPE has yet to be reported (60,68,69). Until such methods are developed, the best suitable point for an RO-RPE merger to obtain more mature OSs from a short-term coculture remains to be detected. During human embryological development, photoreceptor and RPE precursors come into spatial proximity by day 32 (reviewed in (6)). Su et al. used 18-day-old organoids and cocultured them for 30 days (104). Usually, the first photoreceptors emerge in ROs during the seventh differentiation week (60). It is possible that coculture with young organoids significantly improved OS development, but this study did not investigate it. Akhtar et al. observed a significant increase in photoreceptor markers in ROs aged 6-7 weeks and 22-24 weeks that had been cocultured with RPE for 14 days (76). It is interesting to note that this effect on the expression of photoreceptor markers eventually became insignificant when compared to the control group. Achberger et al. cocultured ROs that were approximately 180 days old (77). They confirmed the benefits of photoreceptor-RPE connection for this developmental stage.

In our protocol, ROs are not isolated until the differentiation week 4, and bRPE need several more weeks to acquire maturation. Consequently, our ROs were 105 or 126 days old on day 0 of the coculture experiments. We could consider using cryopreserved and thawed RPE cells to establish a coculture earlier in RO development. Still, if we do, we will miss out on the benefits of simultaneous differentiation of RO and bRPE. Moreover, the studies discussed above show that even older photoreceptors could profit from the connection with RPE. It is possible that RO photoreceptors would benefit from the coculture at every stage of differentiation, as they depend on RPE during their entire lifespan *in vivo*. Still, comparing the influence of the RO-RPE coculture at various developmental stages of photoreceptors would be an exciting investigation.

Apart from coculture with RPE, other adaptations to RO differentiation protocols have been proposed to enhance photoreceptor development, such as supplementing RO medium with RA (74,75,107). In a recently published paper, the authors modified the RO feeding medium, including antioxidants and lipids (107). Under these conditions, abundant and significantly longer OSs were observed in rods and cones. Moreover, the correct stacking of the OS membrane discs was enhanced. Combining these protocol modifications with RPE coculture

could promote photoreceptor maturation in ROs, thus broadening their scientific applications as an RP model.

This study aimed to improve the maturation of photoreceptors in ROs to enhance their potential as a scientific model for RP. For this purpose, we attempted to create a straightforward and effective coculture technique with RPE cells. All three experiments evaluated in this thesis successfully reunited ROs with bRPE cells. Each method provided certain advantages and disadvantages discussed above. In the adherent coculture, the bRPE cells seemed to have phagocyted the shed photoreceptor OSs, a crucial interaction between these two cell types *in vivo*. Nevertheless, the ROs detached from the bRPE, which hindered the investigation of the contact site between them. Unfortunately, we were unable to achieve our ultimate goal of demonstrating any improvement in OS development in our cocultures. Still, a reproducible method to generate RPE from the RO differentiation protocol was established in this project, thereby laying the groundwork for future coculture experiments.

In addition to the bRPE differentiation and modeling coculture approaches, this thesis also focused on establishing an *RP1*-knockout hiPSC line. Previously, CRISPR/Cas9 technology was used to induce DNA alterations in exon 2 of the *RP1* gene in hiPSCs (Figure 11A) (69). We analyzed the DNA of the hiPSC single clones via Sanger sequencing. As a result, a novel homozygous single-base insertion was detected in one clone (Figure 11B). This mutation was predicted to lead to a premature stop codon in exon 2. It was postulated that truncated *RP1*-mRNA would be degraded through nonsense-mediated decay (reviewed in (45)), resulting in the absence of the RP1 protein in the hiPSCs.

An intriguing experiment would be to differentiate ROs from the identified clone and investigate their photoreceptors. An expected benefit of using CRISPR/Cas9 instead of hiPSCs from a patient with an *RP1* mutation is minimizing the impact of inter-cell line variability on future RO differentiations. Previously, it was shown that the *RP1* gene is essential for the correct stalking of OS membrane discs (47). As OSs in ROs rarely show correctly stacked membrane discs (60,61), it would be hard to distinguish the influence of the *RP1* phenotype from the often-described drawback of RO differentiation. For this reason, our research and many others seek to enhance the correct organization of photoreceptor OSs in ROs.

During further experiments at the institute, ROs were differentiated from two *RP1*-knockout hiPSC clones (69). No differences were found in the expression of rhodopsin and recoverin between control and *RP1*-knockout ROs in the evaluated immunofluorescent stainings of 6-month-old samples. One possible explanation for these results could be that *RP1*-associated RP develops later in an individual's life (reviewed in (28)). Hence, a longer culturing

time may be required to observe distinctions in photoreceptor development. Future research may involve analyzing photoreceptor morphology and protein expression in *RP1*-knockout ROs older than six months.

7 Summary

The discovery of hiPSC-derived ROs provided a new avenue for retinal research to scientists worldwide. ROs are a unique model system composed of main neuroretinal cell types with a similar structure to the native tissue. However, they have notable drawbacks, including underdeveloped photoreceptor OSs and the lack of physiological contact between photoreceptors and RPE cells. Consequently, the applications of ROs as a model for disorders affecting photoreceptor-RPE system, such as RP, are restricted.

The objective of this thesis was to discover effective methods to overcome this constraint. The RO differentiation protocol was modified to produce RPE cells (bRPE) as a byproduct. This involved extended culturing of the hiPSCs that had not matured into ROs, using nicotinamide to promote RPE development. The adapted protocol was tested in multiple differentiations of three hiPSC lines derived from healthy donors. The bRPE cells exhibited typical RPE morphology and characteristic protein expression in immunofluorescent stainings. In qRT-PCR analysis, three RPE markers were significantly upregulated compared to undifferentiated hiPSCs. Based on the results, it can be concluded that the modified differentiation protocol successfully and consistently produced RPE cells.

This thesis evaluated two approaches to coculture ROs with bRPE cells, intending to promote physical contact between photoreceptors and bRPE. Two coculture experiments were conducted in suspension while testing the first method. Many bRPE cells detached from the RO surface within a few days despite close contact being established between them. A second approach involved culturing under adherent conditions. In this experiment, the bRPE cells were grown as a monolayer on transwell filter inserts. ROs temporarily adhered to the bRPE but detached during harvest. Still, cocultured bRPE stained positive for rhodopsin, a photoreceptor OS marker, providing evidence of a functional connection between the two. Although our experiments did not show an improved OS structure in cocultures, they confirmed a physiological interaction between ROs and bRPE. This provides a solid foundation for future RO-RPE coculture experiments.

Finally, this study investigated hiPSC clones treated with CRISPR/Cas9 to induce novel mutations in the *RP1* gene. Mutations in the *RP1* gene often lead to RP, a genetic condition linked to the degeneration of photoreceptors. One hiPSC clone was found to carry a novel homozygous mutation, which is believed to result in the *RP1*-knockout phenotype. Future differentiation of ROs from this hiPSC clone may provide a framework for studying the functions of the RP1 protein and RP pathogenesis.

8 List of Abbreviations

Abbreviation	Full form
2D	two-dimensional
3D	three-dimensional
ADP	adenosine diphosphate
AIPL1	aryl hydrocarbon receptor-interacting protein-like 1
ARL3	ADP ribosylation factor like GTPase 3
ATPase	adenosine-5'-triphosphatase
BEST1	Bestrophin-1
BMP4	bone morphogenetic protein 4
bRPE	byproduct RPE
CB-hiPSCs	cord blood cells-derived hiPSCs
cDNA	complementary DNA
CNA	copy number alteration
CRISPR	clustered regularly interspaced short palindromic repeats
DAPI	4′,6′-diamidino-2-phenylindole
DMEM	Dulbecco's modified eagle medium
DMR	differently methylated region
DMSO	dimethyl sulfoxide
DNA	deoxyribonucleic acid
dNTP	deoxynucleotide triphosphate
DPBS	Dulbecco’s phosphate buffered saline
ECM	extracellular matrix
EDTA	ethylenediaminetetraacetic acid
FBS	fetal bovine serum
GCL	ganglion cell layer
GFR	growth factor reduced
GTPase	guanosine-5’-triphosphate
hESCs	human embryonic stem cells
hiPSCs	human induced pluripotent stem cells
hSSEA3	human stage-specific embryonic antigen 3
ICC	immunocytochemistry
IgG	immunoglobulin G
indel	insertion or deletion
INL	inner nuclear layer
IPL	inner plexiform layer
iPSCs	induced pluripotent stem cells
IRD	inherited retinal disease
IS	inner segment
K-hiPSCs	keratinocytes-derived hiPSCs
Ki67	marker of proliferation Ki-67
LCA	Leber congenital amaurosis
mAb	monoclonal antibody
MITF	microphthalmia-associated transcription factor
NEAA	non-essential amino acid
NFL	nerve fiber layer
NIM	neural induction medium
ONL	outer nuclear layer
OPL	outer plexiform layer

OS	outer segment
pAb	polyclonal antibody
PAM	protospacer adjacent motif
PBMC	peripheral blood mononuclear cells
PBS	Phosphate-buffered saline
PCR	polymerase chain reaction
PFA	paraformaldehyde
PL	photoreceptor layer
PMEL	premelanosome protein
qRT-PCR	quantitative reverse transcriptase polymerase chain reaction
RA	retinoic acid
RDM	retinal differentiation medium
RNA	ribonucleic acid
RO	retinal organoid
RP	retinitis pigmentosa
RP1	retinitis pigmentosa 1 axonemal microtubule associated
RP2	retinitis pigmentosa 2 activator of ARL3 GTPase
RPE	retinal pigment epithelium
RPE65	retinal pigment epithelium-specific 65 kDa protein
sgRNA	single guide RNA
SDS	sodium dodecyl sulfate
Tris	tris(hydroxymethyl)aminomethane
ZO-1	Zonula occludens-1

9 List of Figures

10 List of Tables

11 References

1. Newman E, Reichenbach A. The Muller cell: a functional element of the retina. Trends in Neurosiences [Internet]. 1996 Aug;19(8):307–12. Available from: https://doi.org/10.1016/0166-2236(96)10040-0
2. Kiel JW. Chapter 2, Anatomy. In: The Ocular Circulation [Internet]. San Rafael (CA): Morgan & Claypool Life Sciences; 2010. Available from: https://www.ncbi.nlm.nih.gov/books/NBK53329/
3. Cunha-Vaz J, Bernardes R, Lobo C. Blood-retinal barrier. Eur J Ophthalmol [Internet]. 2011;21(Suppl. 6):S3–9. Available from: https://doi.org/10.5301/EJO.2010.6049
4. Gramage E, Li J, Hitchcock P. The expression and function of midkine in the vertebrate retina. Br J Pharmacol [Internet]. 2014;171(4):913–23. Available from: https://doi.org/10.1111/bph.12495
5. Andreazzoli M, Barravecchia I, De Cesari C, Angeloni D, Demontis GC. Inducible Pluripotent Stem Cells to Model and Treat Inherited Degenerative Diseases of the Outer Retina: 3D-Organoids Limitations and Bioengineering Solutions. Cells [Internet]. 2021 Sep 1;10(9):2489. Available from: https://doi.org/10.3390/cells10092489
6. Quinn PMJ, Wijnholds J. Retinogenesis of the human fetal retina: An apical polarity perspective. Genes (Basel) [Internet]. 2019 Nov;10(12):987. Available from: https://doi.org/10.3390/genes10120987
7. Cepko CL, Austin CP, Yang X, Alexiades M, Ezzeddine D. Cell fate determination in the vertebrate retina. Proc Natl Acad Sci U S A [Internet]. 1996 Jan;93(2):589–95. Available from: https://doi.org/10.1073/pnas.93.2.589
8. Prada C, Puga J, Perez-Mendez L, Lopez R, Ramirez G. Spatial and Temporal Patterns of Neurogenesis in the Chick Retina. European Journal of Neuroscience [Internet]. 1991 Jun;3(6):559–69. Available from: https://doi.org/10.1111/j.1460-9568.1991.tb00843.x
9. Aldiri I, Xu B, Wang L, Chen X, Hiler D, Griffiths L, et al. The Dynamic Epigenetic Landscape of the Retina During Development, Reprogramming, and Tumorigenesis. Neuron [Internet]. 2017 May;94(3):550-568.e10. Available from: https://doi.org/10.1016/j.neuron.2017.04.022
10. Colozza G, Locker M, Perron M. Shaping the eye from embryonic stem cells: Biological and medical implications. World J Stem Cells [Internet]. 2012 [cited 2023 Sep 2];4(8):80–6. Available from: https://doi.org/10.4252/wjsc.v4.i8.80

11. Chen J, Sampath AP. Chapter 14 - Structure and Function of Rod and Cone Photoreceptors. In: Retina [Internet]. Fifth Edit. Elsevier Inc.; 2013. p. 342–59. Available from: https://doi.org/10.1016/B978-1-4557-0737-9.00014-X
12. Purves D, Augustine GJ, Fitzpatrick D, Katz LC, LaMantia AS, McNamara JO, et al. Anatomical Distribution of Rods and Cones. In: Neuroscience [Internet]. Second Edi. Sunderland (MA): Sinauer Associates; 2001. Available from: https://www.ncbi.nlm.nih.gov/books/NBK10848/
13. Ramamurthy V, Cayouette M. Development and disease of the photoreceptor cilium. Clin Genet [Internet]. 2009 Aug;76(2):137–45. Available from: https://doi.org/10.1111/j.1399-0004.2009.01240.x
14. Cote R. Photoreceptor Phosphodiesterase (PDE6): A G-Protein-Activated PDE Regulating Visual Excitation in Rod and Cone Photoreceptor Cells. In: Beavo JA, Francis SH, Houslay MD, editors. Cyclic Nucleotide Phosphodiesterases in Health and Disease [Internet]. First Edit. CRC Press; 2007. p. 165–93. Available from: https://doi.org/10.1201/9781420020847
15. Mannu GS. Retinal phototransduction. Neurosciences (Riyadh) [Internet]. 2014 Oct;19(4):275–80. Available from: http://www.ncbi.nlm.nih.gov/pubmed/25274585
16. Demb JB, Singer JH. Functional Circuitry of the Retina. Annu Rev Vis Sci [Internet]. 2015;1:263–89. Available from: https://doi.org/10.1146/annurev-vision-082114-035334
17. Strauss O. The Retinal Pigment Epithelium in Visual Function. Physiol Rev [Internet]. 2005;85(3):845–81. Available from: https://doi.org/10.1152/physrev.00021.2004
18. Bok D. The retinal pigment epithelium: a versatile partner in vision. J Cell Sci [Internet]. 1993;1993(Supplement_17):189–95. Available from: https://doi.org/10.1242/jcs.1993.Supplement_17.27
19. Naylor A, Hopkins A, Hudson N, Campbell M. Tight Junctions of the Outer Blood Retina Barrier. Int J Mol Sci [Internet]. 2019 Dec 27;21(1):211. Available from: https://doi.org/10.3390/ijms21010211
20. Wimmers S, Karl MO, Strauss O. Ion channels in the RPE. Prog Retin Eye Res [Internet]. 2007 May;26(3):263–301. Available from: https://doi.org/10.1016/j.preteyeres.2006.12.002
21. Marmorstein AD. The Polarity of the Retinal Pigment Epithelium. Traffic [Internet]. 2001;2(12):867–72. Available from: https://doi.org/10.1034/j.1600-0854.2001.21202.x
22. German OL, Buzzi E, Rotstein NP, Rodríguez-Boulan E, Politi LE. Retinal Pigment Epithelial Cells Promote Spatial Reorganization and Differentiation of Retina

Photoreceptors. J Neurosci Res [Internet]. 2008;86(16):3503–14. Available from: https://doi.org/10.1002/jnr.21813

23. Jablonski MM, Tombran-Tink J, Mrazek DA, Iannaccone A. Pigment Epithelium-Derived Factor Supports Normal Development of Photoreceptor Neurons and Opsin Expression after Retinal Pigment Epithelium Removal. Journal of Neuroscience [Internet]. 2000;20(19):7149–57. Available from: https://doi.org/10.1523/JNEUROSCI.20-19-07149.2000
24. Finnemann SC, Chang Y. Photoreceptor-RPE Interactions. In: Tombran-Tink J, Barnstable CJ, editors. Visual Transduction and Non-Visual Light Perception [Internet]. Humana Press Inc.; 2008. p. 67–86. Available from: https://doi.org/10.1007/978-1-59745-374-5
25. Motta FL, Martin RP, Filippelli-Silva R, Salles MV, Ferraz Sallum JM. Relative frequency of inherited retinal dystrophies in Brazil. Sci Rep [Internet]. 2018 Oct;8:15939. Available from: https://doi.org/10.1038/s41598-018-34380-0
26. Holtan JP, Selmer KK, Heimdal KR, Bragadóttir R. Inherited retinal disease in Norway – a characterization of current clinical and genetic knowledge. Acta Ophthalmol [Internet]. 2020;98(3):286–95. Available from: https://doi.org/10.1111/aos.14218
27. De Roach JN, Mclaren TL, Paterson RL, O'Brien EC, Hoffmann L, Mackey DA, et al. Establishment and evolution of the Australian Inherited Retinal Disease Register and DNA Bank. Clin Exp Ophthalmol [Internet]. 2013;41(5):476–83. Available from: https://doi.org/10.1111/ceo.12020
28. Verbakel SK, van Huet RAC, Boon CJF, den Hollander AI, Collin RWJ, Klaver CCW, et al. Non-syndromic retinitis pigmentosa. Prog Retin Eye Res [Internet]. 2018 Sep;66:157–86. Available from: https://doi.org/10.1016/j.preteyeres.2018.03.005
29. Cross N, van Steen C, Zegaoui Y, Satherley A, Angelillo L. Retinitis Pigmentosa: Burden of Disease and Current Unmet Needs. Clinical Ophthalmology [Internet]. 2022 Jun 20;16:1993–2010. Available from: https://doi.org/10.2147/OPTH.S365486
30. Fahim A. Retinitis pigmentosa: recent advances and future directions in diagnosis and management. Curr Opin Pediatr [Internet]. 2018 Dec;30(6):725–33. Available from: http://journals.lww.com/00008480-201812000-00006
31. Wu KY, Kulbay M, Toameh D, Xu AQ, Kalevar A, Tran SD. Retinitis Pigmentosa: Novel Therapeutic Targets and Drug Development. Pharmaceutics [Internet]. 2023 Feb 17;15(2):685. Available from: http://dx.doi.org/10.3390/pharmaceutics15020685

32. Haim M. The epidemiology of retinitis pigmentosa in Denmark. Acta Ophthalmol Scand [Internet]. 2002 Feb 12;80:1–34. Available from: https://doi.org/10.1046/j.1395-3907.2002.00001.x
33. Puech B, De Laey JJ. Retinitis Pigmentosa and Allied Disorders. In: Puech B, De Laey JJ, Holder GE, editors. Inherited Chorioretinal Dystrophies: A Textbook and Atlas [Internet]. 1st ed. Springer-Verlag Berlin Heidelberg; 2014. p. 99–120. Available from: https://link.springer.com/book/10.1007/978-3-540-69466-3
34. Novak-Lauš K, Kukulj S, Zorić-Geber M, Bastaić O. Primary tapetoretinal dystrophies as the cause of blindness and impaired vision in the republic of Croatia. Acta Clin Croat [Internet]. 2002 Jan;41(1):23–7. Available from: https://hrcak.srce.hr/file/22465
35. Bunker CH, Berson EL, Bromley WC, Hayes RP, Roderick TH. Prevalence of retinitis pigmentosa in Maine. Am J Ophthalmol [Internet]. 1984 Mar;97(3):357–65. Available from: https://doi.org/10.1016/0002-9394(84)90636-6
36. SP Daiger, BJF Rossiter, J Greenberg, A Christoffels WH. Data services and software for identifying genes and mutations causing retinal degeneration. Invest OphthalmolVis Sci. 1998;39:295. Available from: https://sph.uth.edu/RetNet
37. Martin-Merida I, Aguilera-Garcia D, Fernandez-San Jose P, Blanco-Kelly F, Zurita O, Almoguera B, et al. Toward the Mutational Landscape of Autosomal Dominant Retinitis Pigmentosa: A Comprehensive Analysis of 258 Spanish Families. Invest Ophthalmol Vis Sci [Internet]. 2018 May;59(6):2345–54. Available from: https://doi.org/10.1167/iovs.18-23854
38. Sullivan LS, Bowne SJ, Birch DG, Hughbanks-Wheaton D, Heckenlively JR, Lewis RA, et al. Prevalence of Disease-Causing Mutations in Families with Autosomal Dominant Retinitis Pigmentosa: A Screen of Known Genes in 200 Families. Invest Ophthalmol Vis Sci [Internet]. 2006 Jul;47(7):3052–64. Available from: https://doi.org/10.1167/iovs.05-1443
39. Sullivan LS, Heckenlively JR, Bowne SJ, Zuo J, Hide WA, Gal A, et al. Mutations in a novel retina-specific gene cause autosomal dominant retinitis pigmentosa. Nat Genet [Internet]. 1999 Jul;22:255–9. Available from: https://doi.org/10.1038/10314
40. Van Cauwenbergh C, Coppieters F, Roels D, De Jaegere S, Flipts H, De Zaeytijd J, et al. Mutations in Splicing Factor Genes Are a Major Cause of Autosomal Dominant Retinitis Pigmentosa in Belgian Families. PLoS One [Internet]. 2017 Jan;12(1):e0170038. Available from: https://doi.org/10.1371/journal.pone.0170038

41. Siemiatkowska AM, Astuti GDN, Arimadyo K, den Hollander AI, Faradz SMH, Cremers FPM, et al. Identification of a novel nonsense mutation in RP1 that causes autosomal recessive retinitis pigmentosa in an Indonesian family. Mol Vis [Internet]. 2012 Oct;18:2411–9. Available from: http://www.molvis.org/molvis/v18/a254

42. Ferrari S, Di Iorio E, Barbaro V, Ponzin D, Sorrentino FS, Parmeggiani F. Retinitis Pigmentosa: Genes and Disease Mechanisms. Curr Genomics [Internet]. 2011 Jun;12(4):238–49. Available from: https://www.ncbi.nlm.nih.gov/pmc/articles/PMC3131731/

43. Verbakel SK, Van Huet RAC, Den Hollander AI, Geerlings MJ, Kersten E, Klevering BJ, et al. Macular Dystrophy and Cone-Rod Dystrophy Caused by Mutations in the RP1 Gene: Extending the RP1 Disease Spectrum. Invest Ophthalmol Vis Sci [Internet]. 2019 Mar;60(4):1192–203. Available from: https://doi.org/10.1167/iovs.18-26084

44. Payne A, Vithana E, Khaliq S, Hameed A, Deller J, Abu-Safieh L, et al. RP1 Protein Truncating Mutations Predominate at the RP1 adRP Locus. Invest Ophthalmol Vis Sci [Internet]. 2000 Dec;41(13):4069–73. Available from: https://iovs.arvojournals.org/article.aspx?articleid=2162724

45. Chang YF, Imam JS, Wilkinson MF. The Nonsense-mediated Decay RNA Surveillance Pathway. Annu Rev Biochem [Internet]. 2007 Jul;76:51–74. Available from: https://doi.org/10.1146/annurev.biochem.76.050106.093909

46. Zhang J, Sun X, Qian Y, LaDuca JP, Maquat LE. At Least One Intron Is Required for the Nonsense-Mediated Decay of Triosephosphate Isomerase mRNA: a Possible Link between Nuclear Splicing and Cytoplasmic Translation. Mol Cell Biol [Internet]. 1998;18(9):5272–83. Available from: https://doi.org/10.1128/MCB.18.9.5272

47. Liu Q, Lyubarsky A, Skalet JH, Pugh EN, Pierce EA. RP1 Is Required for the Correct Stacking of Outer Segment Discs. Invest Ophthalmol Vis Sci [Internet]. 2003 Oct;44(10):4171–83. Available from: https://doi.org/10.1167/iovs.03-0410

48. Liu Q, Zhou J, Daiger SP, Farber DB, Heckenlively JR, Smith JE, et al. Identification and Subcellular Localization of the RP1 Protein in Human and Mouse Photoreceptors. Invest Ophthalmol Vis Sci [Internet]. 2002 Jan;43(1):22–32. Available from: https://iovs.arvojournals.org/article.aspx?articleid=2123580

49. Liu Q, Zuo J, Pierce EA. The Retinitis Pigmentosa 1 Protein Is a Photoreceptor Microtubule- Associated Protein. Journal of Neuroscience [Internet]. 2004 Jul;24(29):6427–36. Available from: https://doi.org/10.1523/JNEUROSCI.1335-04.2004

50. Artero Castro A, Rodríguez Jimenez FJ, Jendelova P, Erceg S. Deciphering Retinal Diseases Through the Generation of Three-Dimensional Stem Cell-Derived Organoids: Concise Review. Stem Cells [Internet]. 2019 Dec;37(12):1496–504. Available from: https://doi.org/10.1002/stem.3089

51. Murali A, Ramlogan-Steel CA, Andrzejewski S, Steel JC, Layton CJ. Retinal explant culture: A platform to investigate human neuro-retina. Clin Exp Ophthalmol [Internet]. 2019 Mar;47(2):274–85. Available from: https://doi.org/10.1111/ceo.13434

52. Woods S, Taylor K. Ethical and governance challenges in human fetal tissue research. Clin Ethics [Internet]. 2008;3(1):14–9. Available from: https://doi.org/10.1258/ce.2007.007054

53. Takahashi K, Tanabe K, Ohnuki M, Narita M, Ichisaka T, Tomoda K, et al. Induction of Pluripotent Stem Cells from Adult Human Fibroblasts by Defined Factors. Cell [Internet]. 2007 Nov;131(5):861–72. Available from: https://doi.org/10.1016/j.cell.2007.11.019

54. Yu J, Vodyanik MA, Smuga-Otto K, Antosiewicz-Bourget J, Frane JL, Tian S, et al. Induced Pluripotent Stem Cell Lines Derived from Human Somatic Cells. Science [Internet]. 2007 Dec;318(5858):1917–20. Available from: https://www.science.org/doi/10.1126/science.1151526

55. Osakada F, Jin ZB, Hirami Y, Ikeda H, Danjyo T, Watanabe K, et al. In vitro differentiation of retinal cells from human pluripotent stem cells by small-molecule induction. J Cell Sci [Internet]. 2009 Sep;122(17):3169–79. Available from: https://doi.org/10.1242/jcs.050393

56. Krohne TU, Westenskow PD, Kurihara T, Friedlander DF, Lehmann M, L. DA, et al. Generation of Retinal Pigment Epithelial Cells from Small Molecules and OCT4 Reprogrammed Human Induced Pluripotent Stem Cells. Stem Cells Transl Med [Internet]. 2012 Feb;1(2):96–109. Available from: https://doi.org/10.5966/sctm.2011-0057

57. Paşca AM, Sloan SA, Clarke LE, Tian Y, Makinson CD, Huber N, et al. Functional cortical neurons and astrocytes from human pluripotent stem cells in 3D culture. Nat Methods [Internet]. 2015 Jul;12(7):671–8. Available from: https://www.nature.com/articles/nmeth.3415

58. Paşca SP. The rise of three-dimensional human brain cultures. Nature [Internet]. 2018 Jan;553:437–45. Available from: https://www.nature.com/articles/nature25032

59. Eiraku M, Takata N, Ishibashi H, Kawada M, Sakakura E, Okuda S, et al. Self-organizing optic-cup morphogenesis in three-dimensional culture. Nature [Internet]. 2011 Apr;472(7341):51–8. Available from: https://www.nature.com/articles/nature09941
60. Wahlin KJ, Maruotti JA, Sripathi SR, Ball J, Angueyra JM, Kim C, et al. Photoreceptor Outer Segment-like Structures in Long-Term 3D Retinas from Human Pluripotent Stem Cells. Sci Rep [Internet]. 2017 Apr;7(1):776. Available from: https://www.nature.com/articles/s41598-017-00774-9
61. Zhong X, Gutierrez C, Xue T, Hampton C, Vergara MN, Cao LH, et al. Generation of three-dimensional retinal tissue with functional photoreceptors from human iPSCs. Nat Commun [Internet]. 2014 Jun;5:4047. Available from: https://www.nature.com/articles/ncomms5047
62. Phillips MJ, Wallace KA, Dickerson SJ, Miller MJ, Verhoeven AD, Martin JM, et al. Blood-Derived Human iPS Cells Generate Optic Vesicle-Like Structures with the Capacity to Form Retinal Laminae and Develop Synapses. Invest Ophthalmol Vis Sci [Internet]. 2012 Apr;53(4):2007–19. Available from: https://doi.org/10.1167/iovs.11-9313
63. Nakano T, Ando S, Takata N, Kawada M, Muguruma K, Sekiguchi K, et al. Self-Formation of Optic Cups and Storable Stratified Neural Retina from Human ESCs. Cell Stem Cell [Internet]. 2012 Jun;10(6):771–85. Available from: https://doi.org/10.1016/j.stem.2012.05.009
64. Hallam D, Hilgen G, Dorgau B, Zhu L, Yu M, Bojic S, et al. Human-Induced Pluripotent Stem Cells Generate Light Responsive Retinal Organoids with Variable and Nutrient-Dependent Efficiency. Stem Cells [Internet]. 2018 Oct;36(10):1535–51. Available from: https://doi.org/10.1002/stem.2883
65. Lane A, Jovanovic K, Shortall C, Ottaviani D, Panes AB, Schwarz N, et al. Modeling and Rescue of RP2 Retinitis Pigmentosa Using iPSC-Derived Retinal Organoids. Stem Cell Reports [Internet]. 2020 Jul;15(1):67–79. Available from: https://doi.org/10.1016/j.stemcr.2020.05.007
66. Lukovic D, Artero Castro A, Kaya KD, Munezero D, Gieser L, Davó-Martínez C, et al. Retinal Organoids derived from hiPSCs of an AIPL1-LCA Patient Maintain Cytoarchitecture despite Reduced levels of Mutant AIPL1. Sci Rep [Internet]. 2020 Mar;10(1):5426. Available from: https://www.nature.com/articles/s41598-020-62047-2

67. den Hollander AI, Roepman R, Koenekoop RK, Cremers FPM. Leber congenital amaurosis: Genes, proteins and disease mechanisms. Prog Retin Eye Res [Internet]. 2008 Jul;27(4):391–419. Available from: https://doi.org/10.1016/j.preteyeres.2008.05.003

68. Gordon A, Yoon S jin, Tran SS, Makinson CD, Park JY, Andersen J, et al. Long-term maturation of human cortical organoids matches key early postnatal transitions. Nat Neurosci [Internet]. 2021 Mar;24(3):331–42. Available from: https://www.nature.com/articles/s41593-021-00802-y

69. Berber P. Retinal Organoid Differentiation, Characterization, and Adaptation as a Model for Retinitis Pigmentosa [Internet] [Dissertation]. Universität Regensburg; 2022. Available from: https://epub.uni-regensburg.de/53143

70. Völkner M, Zschätzsch M, Rostovskaya M, Overall RW, Busskamp V, Anastassiadis K, et al. Retinal Organoids from Pluripotent Stem Cells Efficiently Recapitulate Retinogenesis. Stem Cell Reports [Internet]. 2016 Apr;6(4):525–38. Available from: https://doi.org/10.1016/j.stemcr.2016.03.001

71. Kaya KD, Chen HY, Brooks MJ, Kelley RA, Shimada H, Nagashima K, et al. Transcriptome-based molecular staging of human stem cell-derived retinal organoids uncovers accelerated photoreceptor differentiation by 9-cis retinal. Mol Vis [Internet]. 2019 Nov;25:663–78. Available from: http://www.molvis.org/molvis/v25/663/

72. Capowski EE, Samimi K, Mayerl SJ, Phillips MJ, Pinilla I, Howden SE, et al. Reproducibility and staging of 3D human retinal organoids across multiple pluripotent stem cell lines. Development [Internet]. 2019 Jan;146(1):dev171686. Available from: https://doi.org/10.1242/dev.171686

73. Ghareeb AE, Lako M, Steel DH. Coculture techniques for modeling retinal development and disease, and enabling regenerative medicine. Stem Cells Transl Med [Internet]. 2020 Dec;9(12):1531–48. Available from: https://doi.org/10.1002/sctm.20-0201

74. Zerti D, Dorgau B, Felemban M, Ghareeb AE, Yu M, Ding Y, et al. Developing a simple method to enhance the generation of cone and rod photoreceptors in pluripotent stem cell-derived retinal organoids. Stem Cells [Internet]. 2020 Jan;38(1):45–51. Available from: https://doi.org/10.1002/stem.3082

75. DiStefano T, Chen HY, Panebianco C, Kaya KD, Brooks MJ, Gieser L, et al. Accelerated and Improved Differentiation of Retinal Organoids from Pluripotent Stem Cells in Rotating-Wall Vessel Bioreactors. Stem Cell Reports [Internet]. 2018 Jan;10(1):300–13. Available from: https://doi.org/10.1016/j.stemcr.2017.11.001

76. Akhtar T, Xie H, Khan MI, Zhao H, Bao J, Zhang M, et al. Accelerated photoreceptor differentiation of hiPSC-derived retinal organoids by contact co-culture with retinal pigment epithelium. Stem Cell Res [Internet]. 2019 Aug;39:101491. Available from: https://doi.org/10.1016/j.scr.2019.101491

77. Achberger K, Probst C, Haderspeck JC, Bolz S, Rogal J, Chuchuy J, et al. Merging organoid and organ-on-a-chip technology to generate complex multi-layer tissue models in a human retina-on-a-chip platform. Elife [Internet]. 2019 Aug;8:e46188. Available from: https://doi.org/10.7554/eLife.46188

78. Walker A, Su H, Conti MA, Harb N, Adelstein RS, Sato N. Non-muscle myosin II regulates survival threshold of pluripotent stem cells. Nat Commun [Internet]. 2010 Sep;1:71. Available from: https://www.nature.com/articles/ncomms1074

79. Müller FJ, Schuldt BM, Williams R, Mason D, Altun G, Papapetrou EP, et al. A bioinformatic assay for pluripotency in human cells. Nat Methods [Internet]. 2011 Apr;8(4):315–7. Available from: https://www.nature.com/articles/nmeth.1580

80. Cowan CS, Renner M, De Gennaro M, Gross-Scherf B, Goldblum D, Hou Y, et al. Cell Types of the Human Retina and Its Organoids at Single-Cell Resolution. Cell [Internet]. 2020 Sep;182(6):1623-1640.e34. Available from: https://doi.org/10.1016/j.cell.2020.08.013

81. Ames JB, Tanaka T, Stryer L, Ikura M. Portrait of a myristoyl switch protein. Curr Opin Struct Biol [Internet]. 1996 Aug;6(4):432–8. Available from: https://doi.org/10.1016/S0959-440X(96)80106-0

82. Hendrickson A, Bumsted-O'Brien K, Natoli R, Ramamurthy V, Possin D, Provis J. Rod photoreceptor differentiation in fetal and infant human retina. Exp Eye Res [Internet]. 2008 Nov;87(5):415–26. Available from: https://doi.org/10.1016/j.exer.2008.07.016

83. Leach LL, Croze RH, Hu Q, Nadar VP, Clevenger TN, Pennington BO, et al. Induced Pluripotent Stem Cell-Derived Retinal Pigmented Epithelium: A comparative Study Between Cell Lines and Differentiation Methods. Journal of Ocular Pharmacology and Therapeutics [Internet]. 2016 Jun;32(5):317–30. Available from: https://doi.org/10.1089/jop.2016.0022

84. Garcia TY, Gutierrez M, Reynolds J, Lamba DA. Modeling the Dynamic AMD-Associated Chronic Oxidative Stress Changes in Human ESC and iPSC-Derived RPE Cells. Invest Ophthalmol Vis Sci [Internet]. 2015 Nov;56(12):7480–8. Available from: https://doi.org/10.1167/iovs.15-17251

85. Idelson M, Alper R, Obolensky A, Ben-Shushan E, Hemo I, Yachimovich-Cohen N, et al. Directed Differentiation of Human Embryonic Stem Cells into Functional Retinal Pigment Epithelium Cells. Cell Stem Cell [Internet]. 2009 Oct 2;5(4):396–408. Available from: https://doi.org/10.1016/j.stem.2009.07.002

86. Singh R, Phillips MJ, Kuai D, Meyer J, Martin JM, Smith MA, et al. Functional Analysis of Serially Expanded Human iPS Cell-Derived RPE Cultures. Invest Ophthalmol Vis Sci [Internet]. 2013 Oct;54(10):6767–78. Available from: https://doi.org/10.1167/iovs.13-11943

87. Brandl C, Zimmermann SJ, Milenkovic VM, Rosendahl SMG, Grassmann F, Milenkovic A, et al. In-depth Characterisation of Retinal Pigment Epithelium (RPE) Cells Derived from Human Induced Pluripotent Stem Cells (hiPSC). Neuromolecular Med [Internet]. 2014 Sep;16(3):551–64. Available from: https://link.springer.com/article/10.1007/s12017-014-8308-8

88. Ortmann D, Vallier L. Variability of human pluripotent stem cell lines. Curr Opin Genet Dev [Internet]. 2017 Oct;46:179–85. Available from: https://doi.org/10.1016/j.gde.2017.07.004

89. Lister R, Pelizzola M, Kida YS, Hawkins RD, Nery JR, Hon G, et al. Hotspots of aberrant epigenomic reprogramming in human induced pluripotent stem cells. Nature [Internet]. 2011 Mar;471(7336):68–73. Available from: https://www.nature.com/articles/nature09798

90. Kim K, Zhao R, Doi A, Ng K, Unternaehrer J, Cahan P, et al. Donor cell type can influence the epigenome and differentiation potential of human induced pluripotent stem cells. Nat Biotechnol [Internet]. 2011 Nov;29(12):1117–9. Available from: https://www.nature.com/articles/nbt.2052

91. Wang L, Hiler D, Xu B, AlDiri I, Chen X, Zhou X, et al. Retinal Cell Type DNA Methylation and Histone Modifications Predict Reprogramming Efficiency and Retinogenesis in 3D Organoid Cultures. Cell Rep [Internet]. 2018 Mar;22(10):2601–14. Available from: https://doi.org/10.1016/j.celrep.2018.01.075

92. Hiler DJ, Barabas ME, Griffiths LM, Dyer MA. Reprogramming of mouse retinal neurons and standardized quantification of their differentiation in 3D retinal cultures. Nat Protoc [Internet]. 2016 Oct;11(10):1955–76. Available from: https://www.nature.com/articles/nprot.2016.109

93. Kilpinen H, Goncalves A, Leha A, Afzal V, Alasoo K, Ashford S, et al. Common genetic variation drives molecular heterogeneity in human iPSCs. Nature [Internet]. 2017 Jun;546(7658):370–5. Available from: https://www.nature.com/articles/nature22403
94. Mayshar Y, Ben-David U, Lavon N, Biancotti JC, Yakir B, Clark AT, et al. Identification and Classification of Chromosomal Aberrations in Human Induced Pluripotent Stem Cells. Cell Stem Cell [Internet]. 2010 Oct;7(4):521–31. Available from: https://doi.org/10.1016/j.stem.2010.07.017
95. Chen KG, Mallon BS, McKay RDG, Robey PG. Human Pluripotent Stem Cell Culture: Considerations for Maintenance, Expansion, and Therapeutics. Cell Stem Cell [Internet]. 2014 Jan;14(1):13–26. Available from: https://doi.org/10.1016/j.stem.2013.12.005
96. Volpato V, Webber C. Addressing variability in iPSC-derived models of human disease: Guidelines to promote reproducibility. Dis Model Mech [Internet]. 2020 Jan;13(1):dmm042317. Available from: https://doi.org/10.1242/dmm.042317
97. Chichagova V, Hilgen G, Ghareeb A, Georgiou M, Carter M, Sernagor E, et al. Human iPSC differentiation to retinal organoids in response to IGF1 and BMP4 activation is line- and method-dependent. Stem Cells [Internet]. 2020 Feb;38(2):195–201. Available from: https://doi.org/10.1002/stem.3116
98. Berber P, Bondarenko S, Michaelis L, Weber BHF. Transient Retention of Photoreceptor Outer Segments in Matrigel-Embedded Retinal Organoids. Int J Mol Sci [Internet]. 2022 Nov;23(23):14893. Available from: https://doi.org/10.3390/ijms232314893
99. Shen CC, Huang HM, Ou HC, Chen HL, Chen WC, Jeng KC. Protective Effect of Nicotinamide on Neuronal Cells under Oxygen and Glucose Deprivation and Hypoxia/Reoxygenation. J Biomed Sci [Internet]. 2004;11(4):472–81. Available from: https://doi.org/10.1159/000077897
100. Regent F, Batz Z, Kelley RA, Gieser L, Swaroop A, Chen HY, et al. Nicotinamide Promotes Formation of Retinal Organoids From Human Pluripotent Stem Cells via Enhanced Neural Cell Fate Commitment. Front Cell Neurosci [Internet]. 2022 Jun;16:878351. Available from: https://doi.org/10.3389/fncel.2022.878351
101. Campochiaro PA, Hackett SF, Conway BP. Retinoic Acid Promotes Density-Dependent Growth Arrest in Human Retinal Pigment Epithelial Cells. Invest Ophthalmol Vis Sci [Internet]. 1991 Jan;32(1):65–72. Available from: https://iovs.arvojournals.org/article.aspx?articleid=2178681

102. Orlando KA, Stone NL, Pittman RN. Rho kinase regulates fragmentation and phagocytosis of apoptotic cells. Exp Cell Res [Internet]. 2006 Jan;312(1):5–15. Available from: https://doi.org/10.1016/j.yexcr.2005.09.012

103. Dorgau B, Felemban M, Hilgen G, Kiening M, Zerti D, Hunt NC, et al. Decellularised extracellular matrix-derived peptides from neural retina and retinal pigment epithelium enhance the expression of synaptic markers and light responsiveness of human pluripotent stem cell derived retinal organoids. Biomaterials [Internet]. 2019 Apr;199:63–75. Available from: https://doi.org/10.1016/j.biomaterials.2019.01.028

104. Su T, Liang L, Zhang L, Wang J, Chen L, Su C, et al. Retinal organoids and microfluidic chip-based approaches to explore the retinitis pigmentosa with USH2A mutations. Front Bioeng Biotechnol [Internet]. 2022 Sep;10:939774. Available from: https://doi.org/10.3389/fbioe.2022.939774

105. Bhattacharya G, Kalluri R, Orten DJ, Kimberling WJ, Cosgrove D. A domain-specific usherin/collagen IV interaction may be required for stable integration into the basement membrane superstructure. J Cell Sci [Internet]. 2004 Jan;117(2):233–42. Available from: https://doi.org/10.1242/jcs.00850

106. Liu X, Bulgakov O V, Darrow KN, Pawlyk B, Adamian M, Charles Liberman M, et al. Usherin is required for maintenance of retinal photoreceptors and normal development of cochlear hair cells. PNAS [Internet]. 2007 Mar;104(11):4413–8. Available from: www.sph.uth.tmc.edu/Retnet

107. West EL, Majumder P, Naeem A, Fernando M, Hara-wright MO, Lanning E, et al. Antioxidant and lipid supplementation improve the development of photoreceptor outer segments in pluripotent stem cell-derived retinal organoids. Stem Cell Reports [Internet]. 2022 Apr;17(4):775–88. Available from: https://doi.org/10.1016/j.stemcr.2022.02.019

12 Eidesstattliche Erklärung

Ich erkläre hiermit, dass ich die vorliegende Arbeit ohne unzulässige Hilfe Dritter und ohne Benutzung anderer als der angegebenen Hilfsmittel angefertigt habe. Die aus anderen Quellen direkt oder indirekt übernommenen Daten und Konzepte sind unter Angabe der Quelle gekennzeichnet. Insbesondere habe ich nicht die entgeltliche Hilfe von Vermittlungs- bzw. Beratungsdiensten, Promotionsberater oder andere Personen in Anspruch genommen.

Niemand hat von mir unmittelbar oder mittelbar geldwerte Leistungen für Arbeit erhalten, die im Zusammenhang mit dem Inhalt der vorgelegten Dissertation stehen.

Die Arbeit wurde bisher weder im In- noch im Ausland in gleicher oder ähnlicher Form einer anderen Prüfungsbehörde vorgelegt.

Regensburg, den 04.01.2024

Sofiia Bondarenko

13 Acknowledgments

First, I want to extend my gratitude to my supervisor Prof. Dr. Bernhard Weber for giving me the chance to work on my medical thesis at the Institute for Human Genetics. Thank you for your dedicated guidance and expertise throughout this project.

I am also grateful to Prof. Dr. Klaus Stark for agreeing to act as the second examiner of this thesis.

I would like to express my profound appreciation to Dr. Dr. Patricia Berber for her unwavering help and support during my time at the institute. I am grateful for your insightful suggestions throughout each stage of this project.

Thanks should go to Lisa Michaelis for sharing her technical expertise in laboratory work with me. I am also thankful to Nico Hertel for providing valuable insights into cell culturing.

I want to extend my sincere thanks to everyone I met at the institute for their support and sharing their experiences with me.

I cannot put into words how grateful I am to my family for their unconditional love and trust in me.

I would like to thank my friend Vlada for her constant support and attentive ear throughout the past few years.

I thank Jerry and Schyla for being there when I needed you.

Lastly, I would not be where I am today without my partner Mateusz. I appreciate your words of encouragement and positivity throughout the entire process. Thank you.